Chemical Engineering and Processing 85 (2014) 256–290

Contents lists available at ScienceDirect

Chemical Engineering and Processing: Process Intensification

journal homepage: www.elsevier.com/locate/cep

Review

Gas–solid fluidized beds in vortex chambers

Juray De Wilde *

Université Catholique de Louvain, Materials and Process Engineering (iMMC–IMAP), Place Sainte Barbe 2, 1348 Louvain-la-Neuve, Belgium

ARTICLE INFO

Article history:
Received 22 January 2014
Received in revised form 7 July 2014
Accepted 31 August 2014
Available online 28 September 2014

Keywords:
High-G fluidization
Vortex chamber
Rotating fluidized bed
Process intensification

ABSTRACT

This review deals with gas–solid fluidized beds in vortex chambers. High-G fluidization can be achieved in a static geometry and allows significant process intensification. Thin, dense and more uniform particle beds can be obtained at high gas–solid slip velocities, intensifying interfacial transfer of mass, heat and momentum and reducing the gas–solid contact time. Existing fluidized bed processes can be carried out more efficiently and novel processing routes can be developed, e.g., involving cohesive particles or a dispersed liquid phase in relatively high concentrations.

The first section of the review discusses the unique hydrodynamic characteristics of gas–solid fluidized beds in vortex chambers. The flow pattern, flexibility in the operating conditions and stability conditions are explained.

The design of vortex chambers is dealt with in the second section and is critical for processing both larger and fine particles. The influence of the gas and solids in- and outlet design is focused on and insight is gained from recent theoretical, experimental and CFD studies.

In the third section (potential) applications are discussed and process intensification and novel processing routes demonstrated. The fourth and last section presents extensions of the concept. Multi-zone operation and the integration of other technologies in vortex chambers are considered.

Contents

* Tel.: +32 10 47 8193; fax: +32 10 47 4028.
E-mail address: Juray.DeWilde@UCLouvain.be (J. De Wilde).

http://dx.doi.org/10.1016/j.cep.2014.08.013
0255-2701/

1. The use of a high-G field for fluidized bed process intensification

Fluidized bed processes are widely applied in refining and in the energy, chemical, pharmaceutical and feed and food industries. Depending on the required gas and solids residence times, the fluidized bed is operated in the bubbling-, turbulent- or transport regime. Fluidized beds are known for their excellent heat transfer properties. Nevertheless, in conventional fluidized beds, the coefficients of interfacial mass, momentum and heat transfer are limited by the value of the gas–solid slip velocity which cannot exceed the terminal or free-fall velocity of the particles in the earth gravitational field [38]. Fine ($<30\,\mu m$) or light cohesive powders can as such not be fluidized, inter-particle Van der Waals forces always dominating interfacial momentum transfer by drag. Furthermore, with increasing gas velocity, the particle bed expands and the solids volume fraction decreases gradually to only a few percent in the riser regime. A uniform distribution of the particles can only be achieved with certain particles and at gas velocities close to the minimum fluidization velocity. In practice, meso-scale bubbles and clusters are formed and their presence is detrimental for gas–solid contact and the related performance of fluidized bed devices. Finally, a certain range of particle bed width-to-height ratios has to be respected to avoid channeling and slugging.

The limitations encountered in conventional fluidized beds can be removed by fluidizing against a high-gravity (high-G) field. Cylindrically shaped rotating fluidized beds have been developed in this context. The radial fluidization of the particle bed is controlled by balancing the drag force exerted by a radially inwards flowing gas and the particle inertial forces. High-G fluidized beds can be operated densely and more uniformly at higher gas–solid slip velocity and as such intensified interfacial transfer of mass, momentum and heat. Furthermore, high-G operation allows working with a high particle bed width-to-height ratio, i.e., thin particle beds, while avoiding channeling. Hence, extremely short gas–solid contact times can be realized which opens perspectives for a variety of industrial processes, the use of more active catalysts, etc.

The necessary rotational motion of rotating fluidized beds can be introduced in different ways. A fluidization chamber rotating around its axis of symmetry can be used, with a motor driving the rotation. Alternatively, a so-called vortex- or whirl chamber can be used, which is essentially a static device. The process gas itself then drives the particle bed rotation, the gas being injected tangentially into the vortex chamber via multiple gas inlet slots. When a rotating fluidization chamber driven by a motor is used, the particle bed rotation speed can be controlled independently of the gas flow rate, increasing the operating flexibility. Different applications have been considered, such as gas phase polymerization [2] and the production and coating of cohesive powders [73,72,52,53], but scale-up and commercialization of a rotating fluidization chamber were found to be challenging. Vortex chambers do not suffer from a moving geometry, facilitating industrial application. The particle bed rotation speed can, however, no longer be controlled independently of the gas flow rate. This requires a careful vortex chamber design and implies a reduced operating flexibility, e.g., with respect to the type of particles that can be used with a given vortex chamber design. Theoretical studies of rotating fluidized beds in a rotating fluidization chamber can be found in Kroger et al. [45], Chevray et al. [9], Fan et al. [36], Saunders [54], Chen [7], Qian et al. [50,51], and Howley and Pfeffer [41]. This review focuses on gas–solid rotating fluidized beds in vortex chambers, also referred to as rotating fluidized beds in a static geometry (RFB-SG). The hydrodynamic characteristics, design aspects, a number of case studies illustrating the process intensification that can be achieved, and possible extensions of the concept are discussed in separate sections.

2. The generation of rotating fluidized beds in vortex chambers

The use of vortex chambers for the generation of rotating fluidized beds is explained in Fig. 1. The process gas is injected tangentially in the vortex chamber, via multiple gas inlet slots. When introducing particles, they are entrained by the gas. The latter is forced to leave the vortex chamber via a centrally positioned chimney and to flow radially through the particle bed. The particles are unable to follow the gas phase flow path due to their inertia, leading to the formation of a dense rotating particle bed near the cylindrical wall of the vortex chamber and gas–solids separation. Particles can be entrained into the particle bed freeboard region and into the chimney if the radially inwards drag force exceeds the radially outwards centrifugal force. If a particle is radially entrained, the Coriolis effect may allow the particle to convert its radial momentum into tangential momentum and to return to the particle bed. Balancing the radial drag force and the particle inertial forces, i.e., the centrifugal and Coriolis forces requires a careful vortex chamber and chimney design, as discussed later in this review. When continuously feeding solids, independently controlling the gas and particle residence times in the vortex chamber requires a separate solids outlet.

Vortex chambers differ from cyclone chambers [67] and Torbed devices in which a rotating particle bed is suspended on a rotating gas flow [26,56,66,74]. In Torbeds, the gas inlet slots are integrated in the bottom end wall of a cylindrical fluidization chamber and the

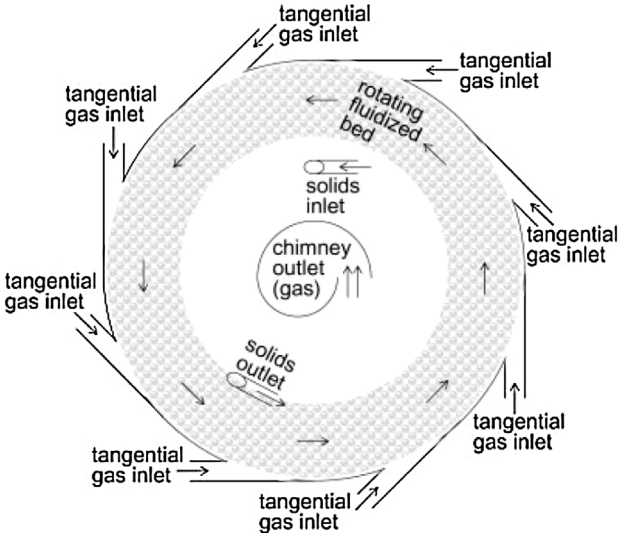

Fig. 1. The generation of a rotating fluidized bed in a static vortex chamber. (From Ref. [20]).

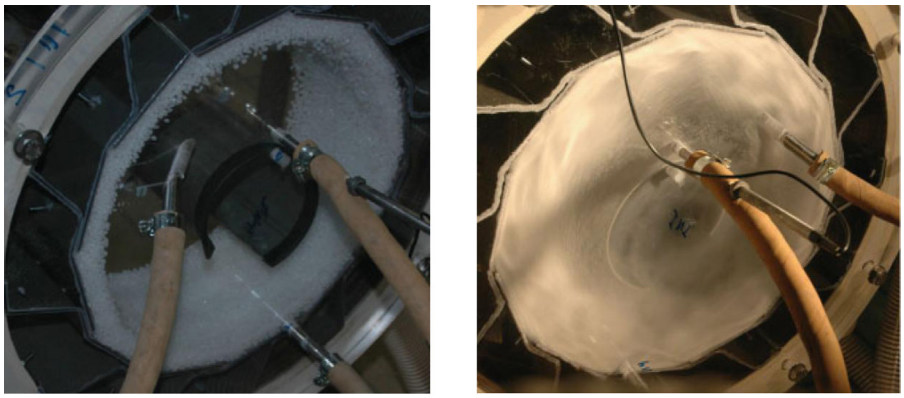

(a) 2-5 mm polymer pellets, 3rps (7G) (b) 300 μm Alumina, (3-4 rps) 10G

Fig. 2. Fluidization of (a) 2–5 mm HDPE polymer pellets and (b) 300 μm alumina in a vortex chamber of given design with $D = 36$ cm, $L = 13.5$ cm, $n = 12$, $s = 4$ mm, $\lambda = 0.042$ and operating at a total gas flow rate of 0.2 Nm^3/s and a solids loading of 1–1.5 kg. Continuous operation with a side solids inlet and outlet. (From Ref. [20]).

gas is forced to leave via the top end wall. Fluidization of the particle bed is essentially not high-G and in the vertical direction against earth gravity.

High-G fluidization of particles in vortex chambers was considered in the late sixties in the context of biomass drying [43,44] and the development of nuclear reactors, e.g., for rockets [3,4,47,60]. Until recently [11–15,71,34], other applications, e.g., in the chemical process industries, were not considered, partially because of a poor understanding of the technology. Gas–liquid- and liquid–solid flows in vortex chambers have been studied by Loftus et al. [48] and Kuzmin et al. [46], respectively, Folsom [37] and Goldshtik et al. [40]. The present review focuses on high-G gas–solid fluidized beds in which the effect of gravity is relatively unimportant. Vortex chambers are typically operated at 5–50G, operation at higher-G requiring extremely high gas flow rates and/or unrealistically small gas inlet slots and introducing high shear in the particle bed which may lead to significant attrition with given types of particles. At sufficient particle bed rotation speed, the vortex chamber can be operated vertically or horizontally. If the effect of earth gravity cannot be completely neglected, vertical or horizontal operation may be preferred. Use can eventually be made of earth gravity, e.g., to introduce an axial motion of the particles.

3. Hydrodynamic characteristics of rotating fluidized beds in vortex chambers

The hydrodynamic characteristics of fluidized beds in vortex chambers are very different from those in conventional fluidized beds. The distinction between tangential and radial fluidization of the particle bed is discussed first, the influence of particles on the flow field next. The operating principle of vortex chambers leads to a remarkable flexibility with respect to the main operating conditions – the gas flow rate and the solids loading, an aspect explained in a third sub-section. In two subsequent sub-sections on large- respectively meso-scale non-uniformities, the stability and uniformity of the particle bed are addressed. Some additional aspects of importance for modeling and practical applications are discussed at the end of this section.

3.1. Tangential and radial fluidization in vortex chambers

Particle beds rotating in vortex chambers are always fluidized. They are, however, not necessarily fluidized in the radial direction. Radial fluidization is dictated by the balance between the radial gas–solid drag force and the particle inertial forces and implies a

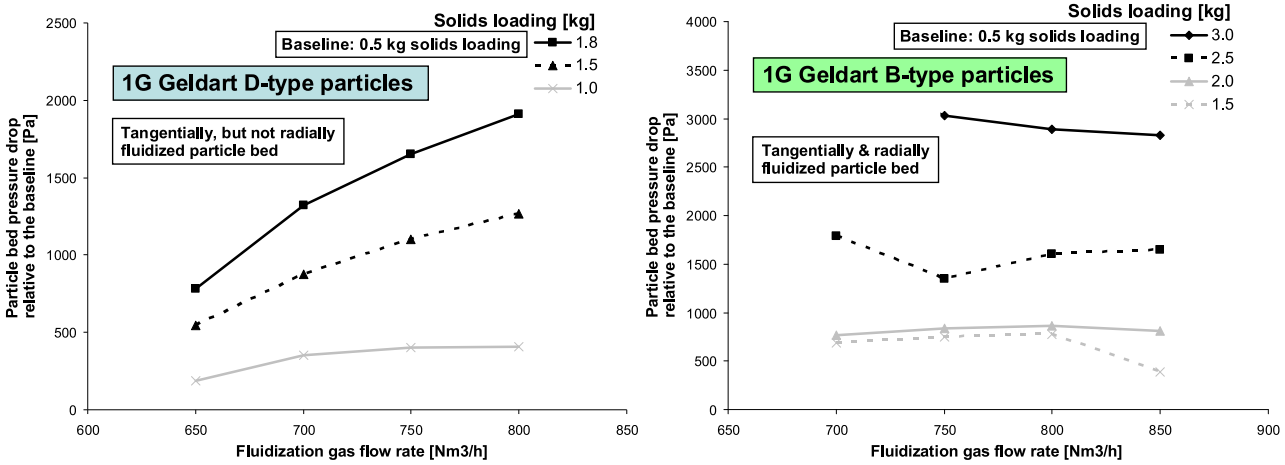

(a) 2-5 mm polymer pellets (b) 300 μm salt

Fig. 3. Fluidization of (a) 2–5 mm HDPE polymer pellets and (b) 300 μm salt in a vortex chamber of given design with $D = 24$ cm, $L = 11.5$ cm, $n = 24$, $s = 2.3$ mm, $\lambda = 0.073$. Pressure drop over the particle bed as a function of the gas flow rate for different solids loadings allowing the detection of radial fluidization. Continuous operation with side solids inlet and chimney outlet.

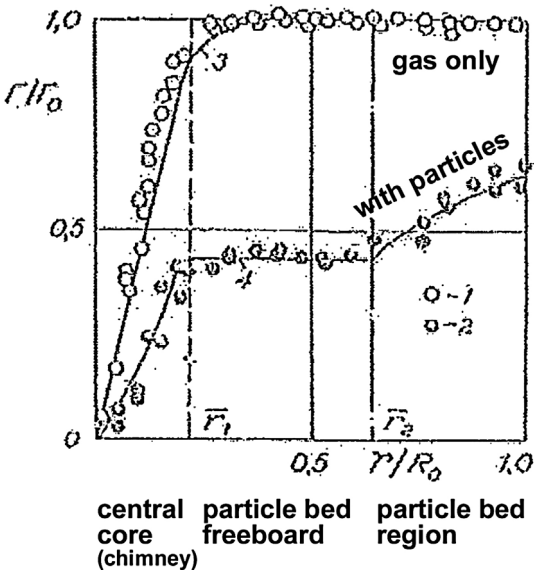

Fig. 4. Influence of the presence of particles on the radial profiles of the circulation ($\Gamma = v_t \times r$, normalized with the value at the outer wall) in a vortex chamber with $D = 36$ cm, $L = 6$ cm, $D_c = 8$ cm, $n > 20$, $\lambda = 0.099$ and a solids loading of 1 kg of sand particles ($\rho_s = 1900$ kg/m^3, $d_p = 2$ mm). (Adapted from Ref. [68]).

decrease of the particle bed density and an increased presence of particles in the freeboard region, resulting in an increased risk of solids losses via the chimney. The force balance mainly depends on the type of particles used and on the vortex chamber design [20,22,55], as will be discussed later. Fig. 2 illustrates the effect of the particle type on the fluidization behavior in a vortex chamber of given design and imposing a given gas flow rate [20]. With the relatively large 1G-Geldart D-type HDPE polymer pellets (1G- vs. high-G classification, see [51]) no radial fluidization of the particle bed was observed and the particles form a so-called concentrated pseudo-fluidized layer (CPL) which is radially packed, but still well-mixed. With the smaller 1G-Geldart B-type alumina, on the other hand, the bed is radially fluidized. The influence of the gas flow rate on the pressure drop over the particle bed reflects and allows detecting radial fluidization (Fig. 3). In the absence of radial fluidization, (Figs. 2(a) and 3(a)) the pressure drop over the particle bed is too small to compensate for the weight of the particle bed in the high-G field and the particle bed is supported by the cylindrical wall of the vortex chamber. Furthermore, the pressure drop over the particle bed increases with increasing gas flow rate, as expected in a packed bed [35]. When radial fluidization occurs (Figs. 2(b) and 3(b)), the pressure drop over the particle bed becomes quasi independent of the gas flow rate, as in a conventional fluidized bed [38]. A similarity between fluidization in vortex chambers and vibrational fluidization was pointed out by Volchkov et al. [69], who demonstrated that during grain drying and cleaning in a vortex chamber, radial fluidization can occur even when the aerodynamic forces are substantially smaller than the centrifugal force. The importance of this effect depends on the particle type. A criterion for vibrational fluidization was adapted for application to vortex chambers.

In rotating chambers, layered radial fluidization of the particle bed is reported [7]. The phenomenon is explained by the solid body type motion of the bed and the increase of the radial flow velocity towards the central axis of the chamber. As a result, starting from a packed bed, the inner portion of the bed fluidizes first when increasing the gas flow rate. In static vortex chambers, the bed no longer behaves like a solid body, in particular when radially fluidized. A behavior between solid body and free vortex type is observed. Finally, the gas flow rate affects both the radial gas–solid drag force and the centrifugal force in similar ways. Hence, bed expansion with increasing gas flow rate is not necessarily observed. These phenomena are discussed in more detail in the next sections.

3.2. On the partial destruction of the free vortex by particles

When operating a vortex chamber without solids, a free vortex type flow pattern is generated, i.e., $\Gamma = u_t \times r = \text{constant}$, except in the central core region where the process gas is evacuated via the chimney and a quasi-solid body type flow pattern develops. This is illustrated in Fig. 4 showing experimental measurements of Γ as a function of the radial position [68,55]. The same figure shows that the presence of 2 mm sand particles drastically changes the flow pattern. Whereas in the particle bed freeboard region, a close to free vortex type flow pattern can be maintained, in the outer, dense particle bed region, a flow pattern between free vortex and solid body type forms [58]. The actual flow pattern in both regions depends on the ratio of the radial gas–solid drag force and the particle inertial forces generated in the vortex chamber and is mainly determined by the vortex chamber design and the type of particles used. This ratio determines the radial fluidization and related bed density, entrainment of particles into the freeboard region and eventual formation of meso-scale non-uniformities, i.e., bubbles [65]. With the relatively large HDPE polymer pellets used in Fig. 2(a), a radially packed bed forms that rotates nearly like a

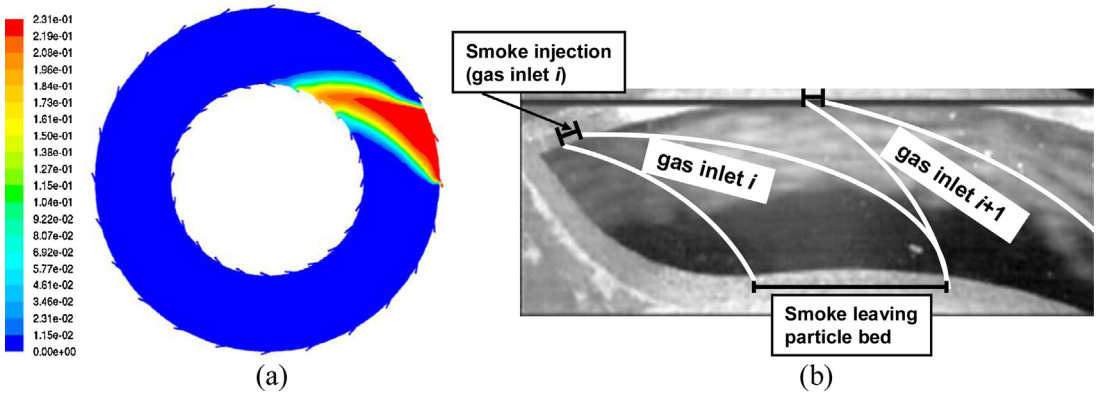

Fig. 5. Tracer study of the gas phase flow path through a rotating bed of particles in a vortex chamber. (a) CFD simulation with a red tracer injected via two of the gas inlet slots. (b) Experimental study with smoke injection via one of the gas inlet slots. Experiments with 2–5 mm 1G-Geldart D-type polymer pellets using a vortex chamber as in Fig. 3. (From Ref. [19]).

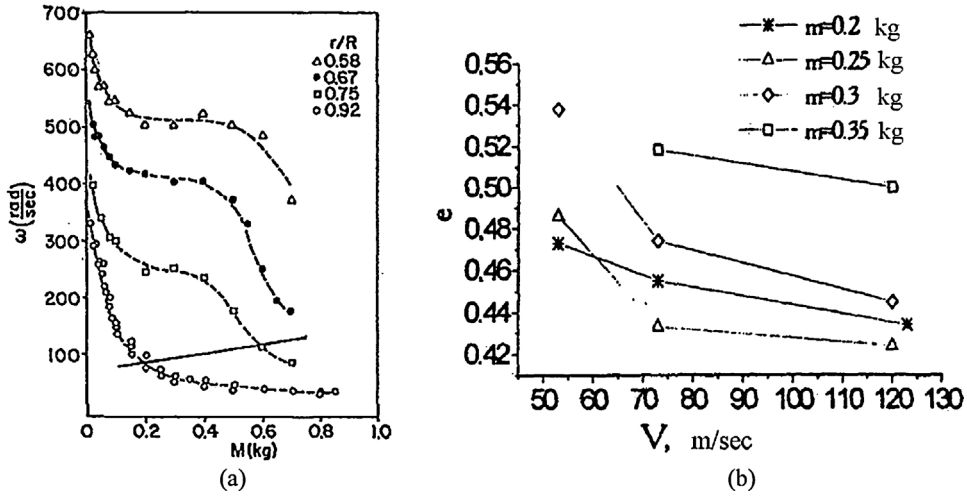

Fig. 6. (a) Variation of the rotation speed at different radial positions with increasing solids loading in a vortex chamber with $D = 30.5$ cm, $L = 6.3$ cm, $D_c = 15 \rightarrow 8$ cm (convergent), $n = 12$, $s = 0.3$ mm, $\lambda = 0.00376$ when fluidizing talc particles ($\rho_s = 2700$ kg/m^3, $d_p = 20$ μm). (From Ref. [4]) (b) Particle bed void fraction as a function of the gas inlet velocity/gas flow rate for different solids loadings in a vortex chamber of given design used for grain drying. (From Ref. [69]).

solid body. No particles are entrained into the freeboard region or chimney. With the smaller alumina particles used in Fig. 2(b), radial fluidization is observed and bubbles form, resulting in a more complex flow pattern. Anderson et al. [4] measured the rotation speed as a function of the solids loading and the position in the vortex chamber when fluidizing small (20 μm) talc particles (Fig. 6(a)). In this case, the bed is less dense and the radial fluidization and entrainment of particles into the freeboard region are pronounced so that there is no clear separation between the dense bed and freeboard regions. As a result, in a certain solids loading range, although the average rotation speed decreases with increasing solids loading, it keeps increasing radially inwards, indicating a flow pattern approaching that of a free vortex. Only at the highest solids loadings, the rotation speeds at different radial positions converge, indicating a gradual transition to a solid body type rotational motion. Finally note that the destruction of the free vortex when introducing particles is reflected in a decrease of the pressure drop over the vortex chamber (see e.g., [24]).

The difference between the gas and solid phase flow patterns in rotating fluidized beds in vortex chambers should be stressed. Although the process gas is injected tangentially, experimental- and CFD tracer studies demonstrate that upon contact with the particle bed it is rapidly tangentially decelerated and deflected radially inwards, as shown in Fig. 5(a and b). When the process gas injected via a given slot approaches the next slot, the radially inwards deflection is boosted. Mixing between gases injected via successive slots is as such limited, opening perspectives for certain applications and multi-zone operation, discussed in Section 6.

3.3. Operating flexibility: influence of the gas flow rate and the solids loading

Because in vortex chambers the particle bed rotation speed cannot be set independently of the gas flow rate, their design is crucial and depends on the particle properties. With a proper design, i.e., allowing the generation of a dense rotating fluidized bed of a given type of particles, a vortex chamber offers, however, a unique flexibility with respect to the gas flow rate. The reason is found in the gas flow rate affecting the radial gas–solid drag force and the counteracting centrifugal force in similar ways. Indeed, when increasing the gas flow rate, the radial gas–solid drag force is obviously increased, but so is the centrifugal force, the particle bed rotational motion being driven by the gas. Depending on the vortex chamber design and the operating conditions, in particular the type of particles fluidized, the increase of the radial gas-solid drag force may be somewhat more or less pronounced than the increase of the centrifugal force, leading to a slight bed expansion, respectively, bed contraction with increasing gas flow rate. At very high gas flow rates, shear grows in importance, the particle bed rotation speed affecting the solid phase viscosity, and the particle bed rotation speed increases less than proportionally with the gas flow rate. Fig. 6(b) shows the variation of the particle bed void fraction (or density) with varying gas flow rate and solids loading in a vortex chamber of given design used for grain drying [69] and illustrates limited bed contraction and densification with increasing gas flow rate in the range studied. Focusing on high-G operation and for a negligible effect of gravity, Sazhin et al. [55] theoretically showed that the retention capacity of vortex chambers, i.e., the amount of solids remaining in the vortex chamber after stopping the solids feeding, is relatively independent of the gas flow rate. This is in agreement with earlier

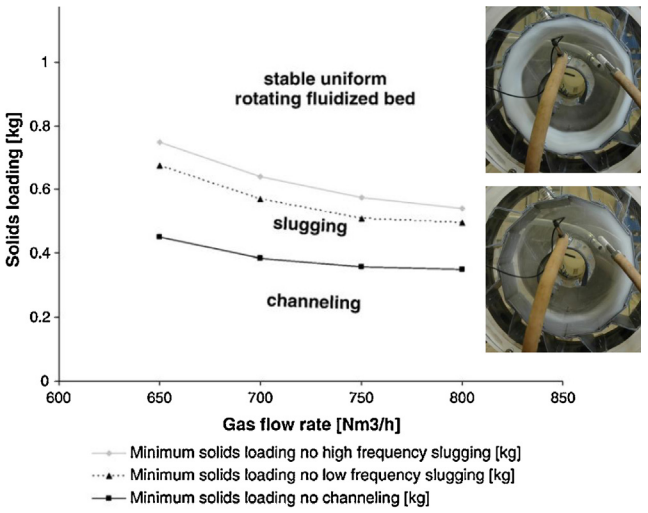

Fig. 7. Flow regime map when fluidizing 2–5 mm HDPE polymer pellets in a vortex chamber of given design with $D = 24$ cm, $L = 13.5$ cm, $n = 24$, $s = 2.3$ mm, $\lambda = 0.073$. Illustrations showing slugging and a stable and uniform bed. At 725 Nm^3/h gas flow rate, the bed was rotating at 4–8 rps (8–31G), for the lowest, respectively, highest solids loading. (Adapted from Ref. [22]).

Fig. 8. High speed CCD camera observations at 1000 frames/s visualizing the formation and motion of bubbles through a bed of 300 μm alumina particles rotating in a vortex chamber. Vortex chamber design as in Fig. 2; camera focusing on a single gas inlet slot. Total gas flow rate: 0.2 m^3/s, solids loading: 1.1 kg, bed rotating at 3.5 rps (10G). (Adapted from Ref. [20]).

experimental observations by Kochetov et al. [43,44] and Anderson et al. [4]. These authors also showed that at low gas flow rates, when the impact of earth gravity cannot be neglected, the retention capacity increases strongly with increasing gas flow rate (see Figs. 12(c) and 13(a) discussed later). De Wilde and de Broqueville [20,22] carried out experiments with continuous solids feeding at given rate and confirmed a minor influence of the gas flow rate on the solids loading in the vortex chamber and on the particle bed stability when working at sufficiently high gas flow rate. The relation between the flexibility in the gas flow rate and the variation of the minimum fluidization- and terminal velocity (radial direction) with the gas flow rate was explained by de Broqueville and De Wilde [16]. Despite this flexibility, rotating fluidized beds in vortex chambers are typically operated at 7–40G (e.g., [20,22,23]) to avoid excessive gas consumption and shear in the particle bed.

Rotating fluidized beds in vortex chambers also offer a certain flexibility with respect to the solids loading. Fig. 6(a) shows the rotation speed as a function of the solids loading for different radial positions in the vortex chamber as measured by Anderson et al. [4]. The rotation speed decreases rapidly when introducing particles in the vortex chamber. This decrease is the most pronounced in the dense particle bed region that is formed ($r/R = 0.92$), but is felt throughout the vortex chamber. When further feeding particles, the particle bed grows without much affecting the rotation speed. A front propagates radially inwards, suggesting the bed grows without causing a significant variation of the bed density. Beyond a certain solids loading, the rotation speed decreases rapidly with increasing solids loading. Anderson et al. [4] explain this by increasing frictional losses arising from the dense peripheral cloud. Trujillo et al. [64] showed that at not too high solids loadings, the dense particle bed region is stabilized and accelerated by the free vortex in the particle lean freeboard region. At high solids loadings, more particles enter the freeboard region and this effect is destroyed. But within a given range, a certain flexibility with respect to the solids loading is demonstrated. The experiments on grain drying by Volchkov et al. [69] shown in Fig. 6(b) confirm this flexibility and a relatively small variation of the particle bed density as the bed grows. Remark that with increasing solids loading, the particle bed density first slightly increases, but then slightly decreases, a clear indication that at high solids loadings shear in the particle bed grows in importance and reduces the particle bed rotation speed. Continuously feeding 1G-Geldart B- and D-type solids in a vortex chamber of given design, De Wilde and de Broqueville [22,23] also demonstrated a certain flexibility with respect to the solids feeding rate and corresponding solids loading. Notice that when measuring the flow characteristics as a function of the solids loading, hysteresis can be observed [23]. De

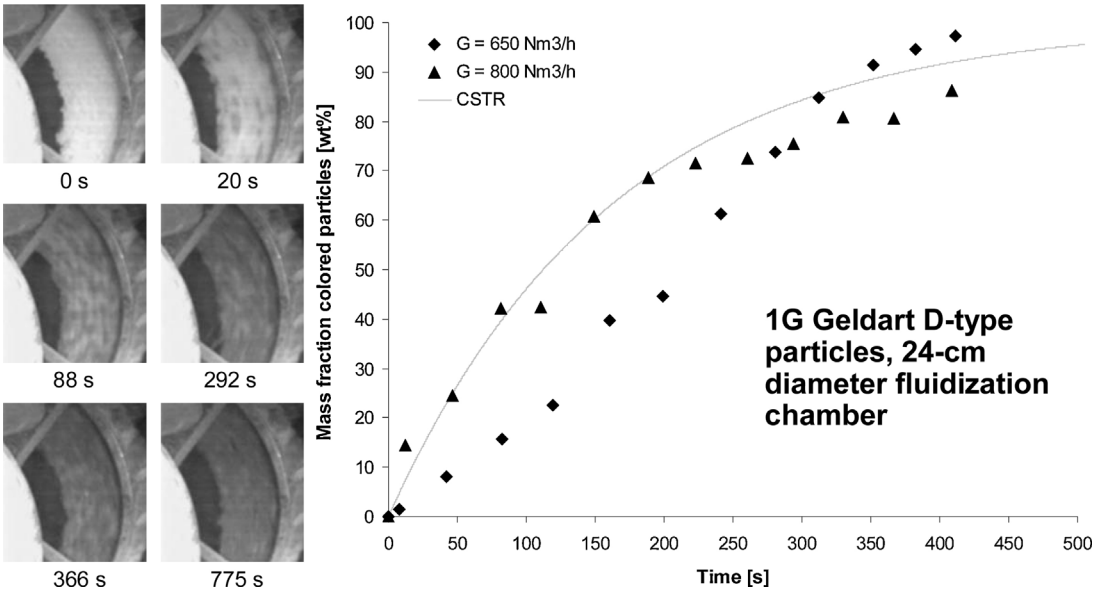

Fig. 9. Step-response study of mixing in a rotating fluidized bed in a vortex chamber using colored particles. Experiments with continuous solids feeding and imposing a step change in the feed particle color at $t = 0$ s from 0 to 100%. Influence of the gas flow rate on the response of the concentration colored particles in the vortex chamber. Theoretical curve illustrates the behavior with a well-mixed particle bed. Experiments with 2–5 mm 1G-Geldart D-type polymer pellets using a vortex chamber as in Fig. 3. (From Ref. [19]).

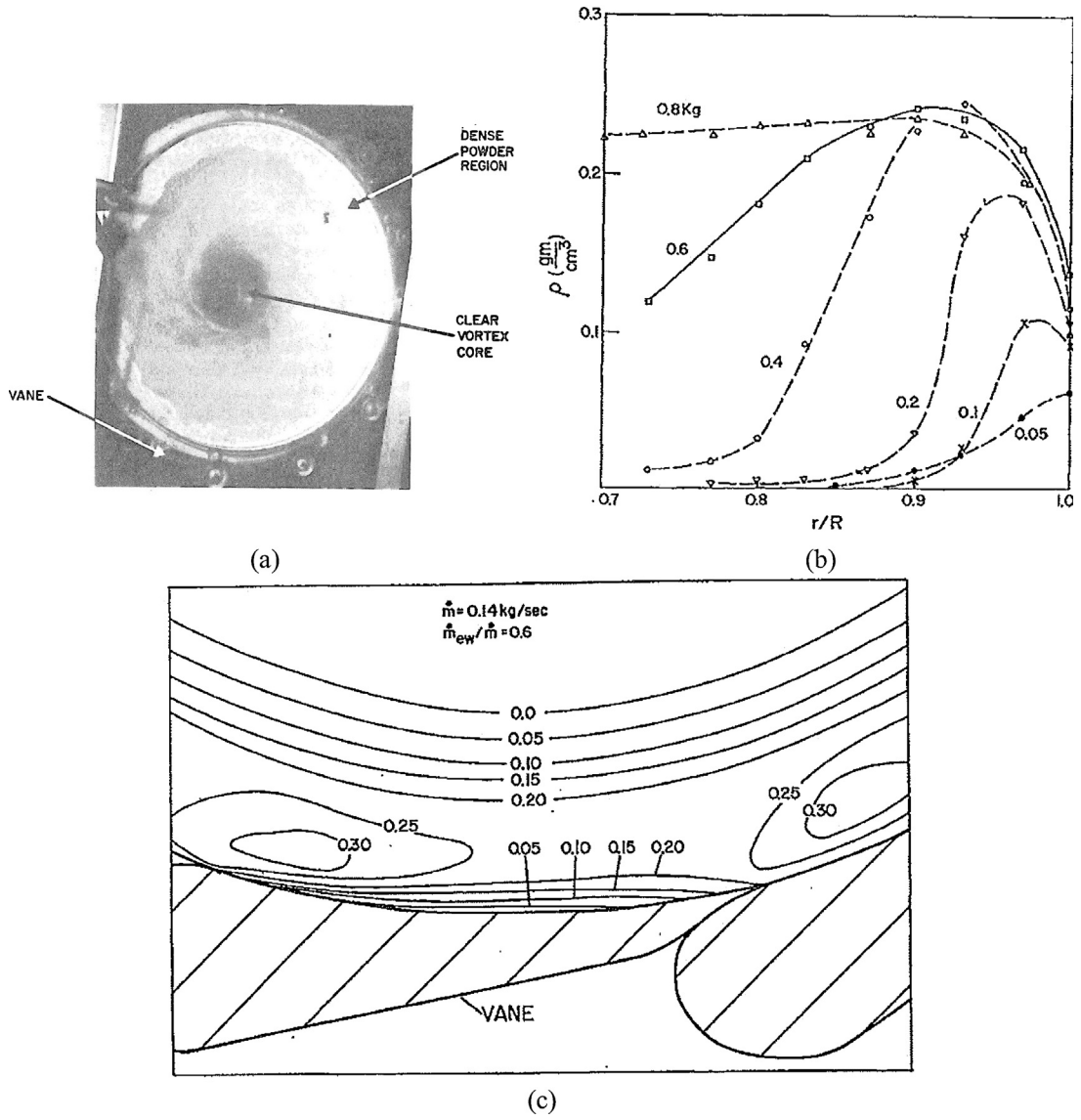

Fig. 10. X-ray absorption measurements (100 kv, 15 ma, typical exposure time: 1 s) during the fluidization of fine talc powder (d_p = 20 μm, ρ_s = 2700 kg/m^3) in a vortex chamber with D = 30.5 cm, L = 6.3 cm, $n \times s$ = 0.36 cm, λ = 0.00376, and operating at a total gas flow rate of 0.117 Nm^3/s and a solids loading of 0.05–0.8 kg. (a) Picture; (b) radial profiles of the axially-, tangentially- and time-averaged particle bed density at different solids loadings; (c) typical particle bed density contours for a solids loading of 0.4 kg. (From Ref. [4]).

Wilde and de Broqueville [20] showed that with a proper vortex chamber design, allowing zero solids losses via the chimney, the gas and solids fluxes can be independently controlled. The full range of gas and solids fluxes in which vortex chambers can be operated requires more detailed studies.

3.4. Particle bed stability and large-scale non-uniformities

As in conventional fluidized beds, large-scale non-uniformities like slugging or channeling can occur in rotating fluidized beds in vortex chambers. They are detrimental for the gas–solid contact and related interfacial transfer of mass, momentum and energy and often for the particle bed stability. Large-scale non-uniformities in the particle bed and in the gas distribution are closely related [65]. In rotating fluidized beds in vortex chambers, only the total gas flow rate is controlled, not the distribution over the different gas inlet slots or the distribution over an individual gas inlet slot, that is, in the axial direction. In their experimental study on the fluidization of 1G-Geldart B- and D-type particles in a vortex chamber of given design, De Wilde and de Broqueville [22] observed that channeling occurs in the axial direction, friction with the end walls playing an important role and causing the process gas to enter preferentially towards the axial center of the vortex chamber. Slugging, on the other hand, implies a strongly non-uniform distribution of the particles in the tangential direction. The particles form a slug which rotates in the vortex chamber, bypassing the process gas that enters mostly via the gas inlet slots not facing the resistance of a particle bed. The flow pattern is then intrinsically non-stationary. Solids losses via the chimney are more pronounced during slugging. If not compensated for by solids feeding, slugging automatically evolves towards channeling. Remark that, studying liquid fluidized beds in vortex chambers, Goldshtik et al. [40] observed condensed stable states and rarefied states of the particle bed, the latter being different with large and small particles.

Focusing on the fluidization of 1G-Geldart D-type particles, De Wilde and de Broqueville [22] mapped the different flow regimes as a function of the gas flow rate and the solids loading in a vortex

chamber of given design. Fig. 7 shows that channeling occurs at low solids loadings, slugging at somewhat higher solids loadings. A stable and uniform rotating fluidized bed requires, however, a sufficiently high solids loading. The vortex chamber design can help achieving this by reducing solids losses via the chimney. The transition from slugging to a stable and uniform rotating fluidized bed regime was observed to be abrupt and results from stresses in the slugging regime become too pronounced so that a stable and uniform rotating fluidized bed is energetically favored. The operating flexibility of vortex chambers with respect to the gas flow rate is reflected in the flow regime map (Fig. 7), the gas flow rate only having a minor impact on the flow regime that is obtained. The length of the vortex chamber can affect the occurrence of large-scale non-uniformities, in particular in the axial direction, i.e., channeling. Although increasing the pressure drop over the gas inlet slots allows improving the uniformity in the vortex chamber (as discussed in more detail in Section 4.1), there are limits to the length that can be used. Testing different vortex chamber designs, Kochetov et al. [43] found that a chamber length below half the chamber diameter was required to guarantee axial particle bed uniformity in the range of operating conditions studied. This was confirmed by more recent experimental data [4,68,20,22,63,34]. The latter also showed that channeling and slugging can occur with smaller Geldart A- and C-type particles. In certain cases, the formation of multiple smaller slugs was observed. Finally, time-accurate pressure measurements at different positions in the vortex chamber and/or the gas distribution chamber allow detecting large-scale non-uniformities [21]. Channeling is reflected in pressure differences along the axial direction, whereas slugging is reflected in temporal pressure fluctuations.

3.5. Particle bed stability and meso-scale non-uniformities

The formation of bubbles is also detrimental for the gas–solid contact and related interfacial transfer of mass, momentum and energy. High-G fluidization allows suppressing bubble formation and improving the particle bed uniformity, at least to a certain extent. Key is the generation of a high hydrostatic pressure drop over the particle bed. This requires a sufficiently high solids loading and particle bed rotation speed in the vortex chamber. Bubble formation is as such affected by the type of particles fluidized and the vortex chamber design. In their investigation of the fluidization behavior of 1G-Geldart B- and D-type particles in a vortex chamber of given design, already referred to in Fig. 2, De Wilde and de Broqueville [20] did not observe any bubble formation with 1G-Geldart D particles, whereas with 1G-Geldart B particles bubble formation was pronounced. Fig. 8 shows high speed CCD camera pictures of the transport of bubbles through the particle bed. Bubbles were seen to form in the vicinity of the gas inlet slots and to propagate both tangentially and radially. In later experimental and numerical studies with 1G-Geldart A- and B-type particles, the impact of the solids loading and of the vortex chamber design on bubble formation and its suppression was demonstrated – see for example Fig. 20 discussed in more detail in Section 4.3 [23,65].

3.6. On the non-ideality of the gas and solid phase flow pattern and distribution and other aspects of importance for practical applications

No simple models are available allowing the accurate calculation of the particle bed rotation speed and related particle bed density and uniformity for given vortex chamber design and operating conditions. CFD models for gas–solid flow have developed since the late sixties and validated through the simulation of conventional fluidized beds and risers [39,57]. Because of the formation of meso-scale phenomena like clusters and bubbles, the flow pattern is intrinsically non-stationary and extremely fine calculation grids are required, resulting in long computation times. The development of filtered gas–solid flow models has been addressed in this context [1]. Specific quantitative validation of CFD models is not possible at this stage due to a lack of data. Qualitative agreement between the experimentally observed and CFD wise calculated behaviors was, however, observed, for example the formation of a dense and uniform or of a bubbling bed for given operating conditions. In the work of Ashcraft et al. [6], discussed in Section 5.4, a Eulerian–Eulerian CFD model was to a certain degree validated, essentially comparing solids loadings in a vortex chamber for given operating conditions. Particle bed rotational speeds were not measured or compared.

When the calculation of the conversion of gas and solid phase species in a vortex chamber reactor is aimed at, an as simple as possible description of the flow pattern can greatly reduce the complexity of the calculations and the calculation time. Fig. 5 shows that in a dense and uniform bed of 1G-Geldart D-type particles, the gas is rapidly deflected in the radial direction after tangential injection in the vortex chamber. Mixing between gases injected via successive inlet slots is minimal. A plug flow assumption for the gas phase may as such be acceptable if the bed is dense and bubble formation can be suppressed. The particle bed may, on the other hand, exhibit a well-mixed behavior, due to the fast particle bed rotational motion, shear and tangential and eventually radial fluidization. This is illustrated in Fig. 9 for a dense and uniform bed of 1G-Geldart D-type particles, showing the response of the concentration of colored particles in the vortex chamber to a step change in the color of the particles fed and this for two different gas flow rates and corresponding particle bed rotation speeds. At sufficiently high particle bed rotation speed, the theoretical response for a well-mixed particle bed is approached. Whether a completely mixed particle bed can be assumed in the presence of reactions depends on a comparison of the mixing- and reaction time scales [38]. In particular, particles have to be able to make multiple turns in the vortex chamber while reacting. Staudt et al. [59] used a reactor model based on plug flow for the gas phase and complete mixing for the particle bed to study the low-

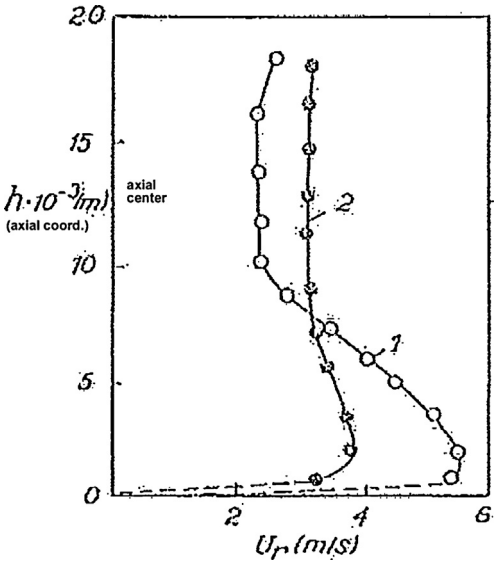

Fig. 11. Axial profiles of the radial gas velocity in the (1) absence and (2) presence (0.15 kg) of particles in a vortex chamber of given design with $D = 20$ cm, $L = 2.6$ cm, $D_c = 10$ cm, $n > 20$, $\lambda = 0.0518$, using wheat grain particles ($\rho_s = 1200$ kg/m^3, $d_p = 2$–5 mm). Illustration of boundary layer flow along the end walls. (Experimental measurements by Volchkov et al. [68]).

Table 1
Experimental studies of gas–solid fluidized beds in vortex chambers. Vortex chamber design and operating conditions.

Ref.	Vortex/distr. chamber diameter (D/D^*) (m)	Chimney diameter (D_c) (m)	Vortex chamber length (L) (m)	Number of gas inlet slots (n)	Gas inlet slot width (s) (m)	$\lambda = n \times s/(\pi \times D)$	Gas flow rate (Q_g) (m^3/s)	Gas phase res. time (T_g) (s)	Gas inlet velocity ($u_{g,in}$) (m/s)	Sup. radial gas velocity ($u_{r,sup}$) ($m^3/(m^2\,s)$)	Particle density (ρ_s) (kg/m^3)	Mean particle diameter (d_p) (m)
[43]	0.12*	0.024–0.096	0.024–0.12	1, 5 (uneven distr.), 6	(6–24)/$n \times 10^{-3}$	0.016–0.0637	0.01–0.028				MSN styrene copolymer ($\neq$ fractions): $\pm$1000	Range: 100E-6–2.50E-03
	0.12*	0.03	0.035	1, 5 (uneven distr.), 6	(6–24)/$n \times 10^{-3}$	0.016–0.0637	0.01–0.028	0.014–0.039		0.76–2.14		
	0.24*	0.048–0.192	0.048–0.24	1, 5 (uneven distr.), 6	(12–48)/$n \times 10^{-3}$	0.016–0.0637	0.01–0.028				quartz sand: 1201	
	0.24*	(0.06)	0.070	1, 5 (uneven distr.), 6	$\cdot 10^{-3}$/$n \times 10^{-3}$	0.016–0.0637	0.01–0.028	0.112–0.315		0.19–0.53	poppy seeds: $\pm$940	
	0.24*	0.06	0.035	1, 5 (uneven distr.), 6	$\cdot 10^{-3}$/$n \times 10^{-3}$	0.0265	0.01–0.028	0.057–0.158		0.38–1.06	millet: $\pm$1000	
	0.44/48* 0.82*	(0.11)	(0.128)	(6)	(0.0034)							
Reported optimum D_c: 0.3–0.5D, chimney entry length: 0.11–0.2L, $L < 0.5$D, and λ: 0.02547–0.03820. Optimum n↑ as d_p↓												
[44]	0.12*	(0.03)	(0.0348)	1, 5 (uneven distr.), 6	/	/	0.01–0.028	0.014–0.039		0.76–2.14	MSN copoly., Sulfanilamide, Melalite, Polystyrene: All $\pm$1050	MSN copoly., Sulfanilamide, Melalite, Polystyrene: 5 fractions: (0.25–0.5)E-3 (0.5–1.0)E-3 (1.2–1.5)E-3 (1.5–2.0)E-3 (2.0–2.5)E-3
	0.24*	(0.06)	(0.035)	1	0.015	0.0199	0.01–0.028	0.057–0.158		0.38–1.06		
	0.24*	(0.06)	(0.035)	5 (u.d.)	0.003	0.0199	0.01–0.028	0.057–0.158		0.38–1.06		
	0.24*	(0.06)	(0.035)	6	0.0025	0.0199	0.01–0.028	0.057–0.158		0.38–1.06		
[4]	0.305	0.15 $\geq$ 0.08 (convergent (second. gas injection)	0.063	12	0.0003	0.0038	0.042–0.15	0.110–0.031	184–661	0.69–2.485	Zinc: 7000	Zinc: 10E-6
											Tungsten: 19100 Talc: 2700	Tungsten: 1.20E-05 Talc: 20E-6
[68]	0.2	0.1 (flat/hyperbolic)	0.026	>20		0.0518	0.046–0.073	0.011–0.018		2.8–4.5	Wheat grain: 1200	Wheat grain: 2-5E-3
[68]	0.36	0.08	0.026	>20		0.0991	0.01–0.1	0.03–0.27		0.34–3.4	Sand: 1900–2000	Sand: (0.2–2.0)E-3
	0.36	0.08 (flat/hyperbolic)	0.06	>20		0.0991	0.01–0.1	0.06–0.61		0.15–1.47	Wheat grain: 1200	Wheat grain: 3.50E-03
											Corn: 1200 Plastic: 1060–1100	Corn: 8.0E-3 Plastic: 3.0E-03
[69]	0.2		0.036			0.0322	0.036–0.051	0.002–0.003	50–70	1.61–2.25	Wheat grain: 1200	Wheat grain: 3.5E-3
[20]	0.36	$\pm$0.12 (slotted with slot size: 0.09 m)	0.135	12	0.004	0.0424	0.2	0.0687	31	1.31	HDPE: cyl.: 950	HDPE: cyl.: d/l = 5/2E-3
											Alumina: 2100	Alumina: (300–400)E-6
[20,22]	0.24	0.15 (slot: 0.08 m, with/out grid)	0.135	12/24	0.0023	0.0366/0.0732	0.2	0.0305	54/27	1.96	HDPE: cyl.: 950	HDPE: cyl.: d/l = 5/2E-3
	0.36	0.12 (slot: 0.09 m)	0.135	12	0.004	0.0424	0.2	0.0687	31	1.31	Salt: 2160	Salt: 350E-6

[23,24]	0.24	0.16 (rotating)	0.115	24	0.0023	0.0732	0.18–0.236	0.022–0.029	28–37	2.08–2.72	HDPE: cyl.: 950 Salt: 2200	HDPE: cyl.: d/l = 5/2E-3 Salt: 350E-6
[28]	(i) 0.26 (ii) 0.26 => 0.23 (iii) 0.23 => 0.2	(i) 0.16	(i) 0.032 (ii) 0.012 (iii) 0.083	(i) 54 (ii) 40 (iii) 40/80	0.0015	(i) 0.0992	(i) ±0.081 (i)+(ii) +(iii) 0.283–0.316	(i) ±0.021	(i) ±31.2	(i) ±3.1	1420	3.50E-03
Comined cylindrical–conical design: (i) upper cylindrical; (ii) transit conical; (iii) lower conical												
[29]	0.54 0.54	0.15 0.15	0.1 0.1	36 36	0.002 0.006	0.042 0.127	0.33–1.0 0.33–1.0	0.023–0.069 0.023–0.069	46–139 15–46	1.95–5.90 1.95–5.90	HDPE: 950 FCC cat.: 1500	HDPE: 3 fractions: 9E-4, 1.6E-3, 2.4E-3 FCC cat.: 70E-6
[63]	0.24 0.24 0.24 0.24 0.24	0.1 0.1 0.1 0.1 0.1	0.05 0.05 0.05 0.05 0.05	24 72 36 72 36	0.003 0.0005 0.0005 0.0002 0.0002	0.0955 0.0477 0.0239 0.0191 0.0096	0.061–0.167 0.061–0.167 0.061–0.167 0.061–0.167 0.061–0.097	0.014–0.037 0.014–0.037 0.014–0.037 0.014–0.037 0.023–0.037	17–46 34–93 68–185 85–232 170–270	1.62–4.42 1.62–4.42 1.62–4.42 1.62–4.42 1.62–2.58	HDPE: 950 Salt: 2160 FCC cat.: 1500	HDPE: 1.0E-03 2.0E-03 Salt: 300E-6 FCC cat.: 7.40E-05
[31,33]	0.43	0.1	0.05	72	0.002	0.1066	0.1944	0.037	27	2.88	600 (dry) 800 (wet)	Pelletized wood: cyl.: d/l = 4/4E-3
[32,34]	0.24	0.1	0.05	72	0.0002	0.0191	0.0694–0.111	0.020–0.033	96–154	1.84–2.95	260	7.00E-05

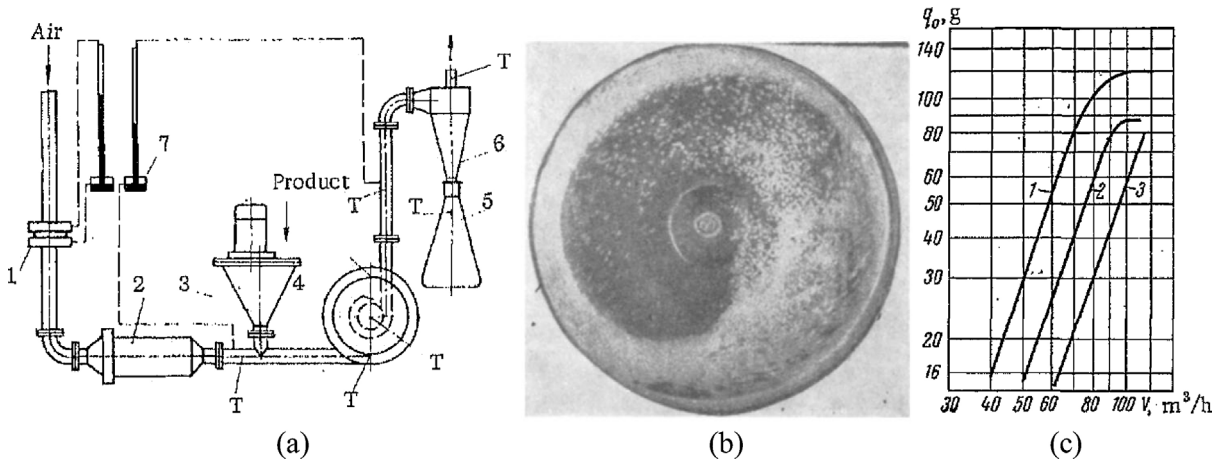

Fig. 12. (a and b): Vortex chamber with a single gas inlet slot through which the gas–solid mixture is tangentially injected. Vortex chamber with $D = 24$ cm, $L = 3.5$ cm, $n \times s = 1.5$ cm, $\lambda = 0.02$. (From Ref. [44]). (c) Solids retention capacity versus air flow rate using three different gas inlet configurations with $n \times s = 2$ cm corresponding to $\lambda = 0.027$. (1) Five gas inlet slots in the lower part of the chamber; (2) one single gas inlet slot; (3) six uniformly distributed gas inlet slots. Other vortex chamber characteristics as in (a and b). (From Ref. [43]).

temperature pyrolysis and gasification of biomass pellets in vortex chambers – see Section 6.

A dense and uniform particle bed is not always obtained, especially with small/light particles. In case the bed is radially fluidized, bubbling can occur and a complex time-averaged particle bed density profile may develop, as already illustrated in Figs. 2 and 8 and confirmed by CFD simulations [65]. Fig. 10 shows X-ray absorption measurements in a rotating fluidized bed of fine talc powder ($d_p = 20$ μm, $\rho_s = 2700$ kg/m^3) in a vortex chamber of given design [4]. Experiments with tungsten ($d_p = 12$ μm, $\rho_s = 19100$ kg/m^3) and zinc ($d_p = 10$ μm, $\rho_s = 7000$ kg/m^3) were also carried out. Radial profiles of the axially-, tangentially- and time-averaged particle bed density at different solids loadings are shown in Fig. 10(b), typical particle bed density contours in Fig. 10(c). Remark that the loosely packed bed density of talc is roughly 0.5 gm/cm^3, so that the bed is relatively dense. Strongly non-uniform particle bed density profiles were observed, both in the radial and tangential direction. With the given type of particles and vortex chamber design, the gas injection is seen to have a pronounced effect on the particle distribution in the vortex chamber. Tangentially averaged, lower bed densities are observed along the cylindrical wall, due to the gas jets entering the chamber. The contours illustrate accumulation of solids upstream of a gas inlet slot, causing radially inward deflection of the gas injected via the previous slot. Reactor models based on idealized flow patterns cannot be used in this case and CFD simulations are required.

In Fig. 10, radial and tangential uniformity of the particle bed was focused on. Axial uniformity is equally important. Section 3.4 dealt with the phenomenon of channeling, an extreme case of axial non-uniformity. The latter is due to friction with the end walls of the vortex chamber, reducing the rotation speed and generating a boundary layer flow. Volchkov et al. [68] measured the axial profiles of the radial gas velocity in a 26 mm long vortex chamber in the absence and presence of 2–5 mm diameter wheat grain

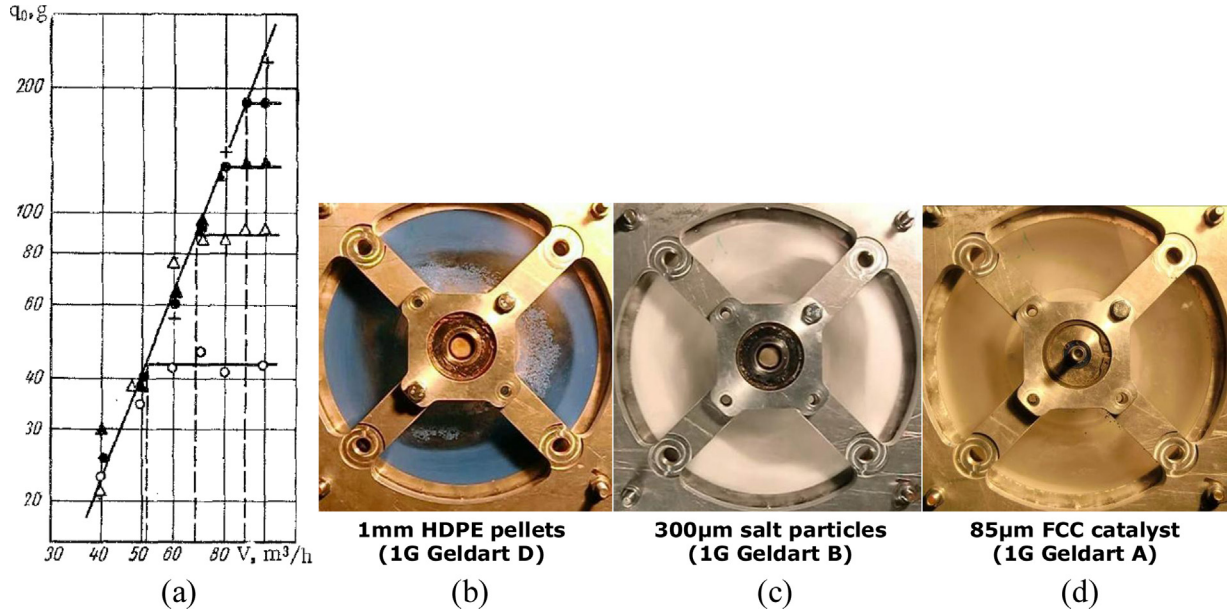

Fig. 13. Fluidization of different size polystyrene particles in a vortex chamber of given design with $D = 24$ cm, $L = 3.5$ cm, $n \times s = 1.5$ cm, $\lambda = 0.02$. (a) Solids retention capacity versus air flow rate with ○ $d_p = 0.25$–0.5 mm; Δ $d_p = 0.5$–1.0 mm; ▲ $d_p = 1.2$–1.5 mm; ● $d_p = 1.5$–2.0 mm. (From Ref. [44]). (b–d) Fluidization at given gas (700 Nm^3/h) and solids (8.35 g/s) feeding rate of different types of particles in a vortex chamber of given design with $D = 24$ cm, $L = 5$ cm, $n = 24$, $s = 3$ mm, $\lambda = 0.096$. (From Ref. [63]).

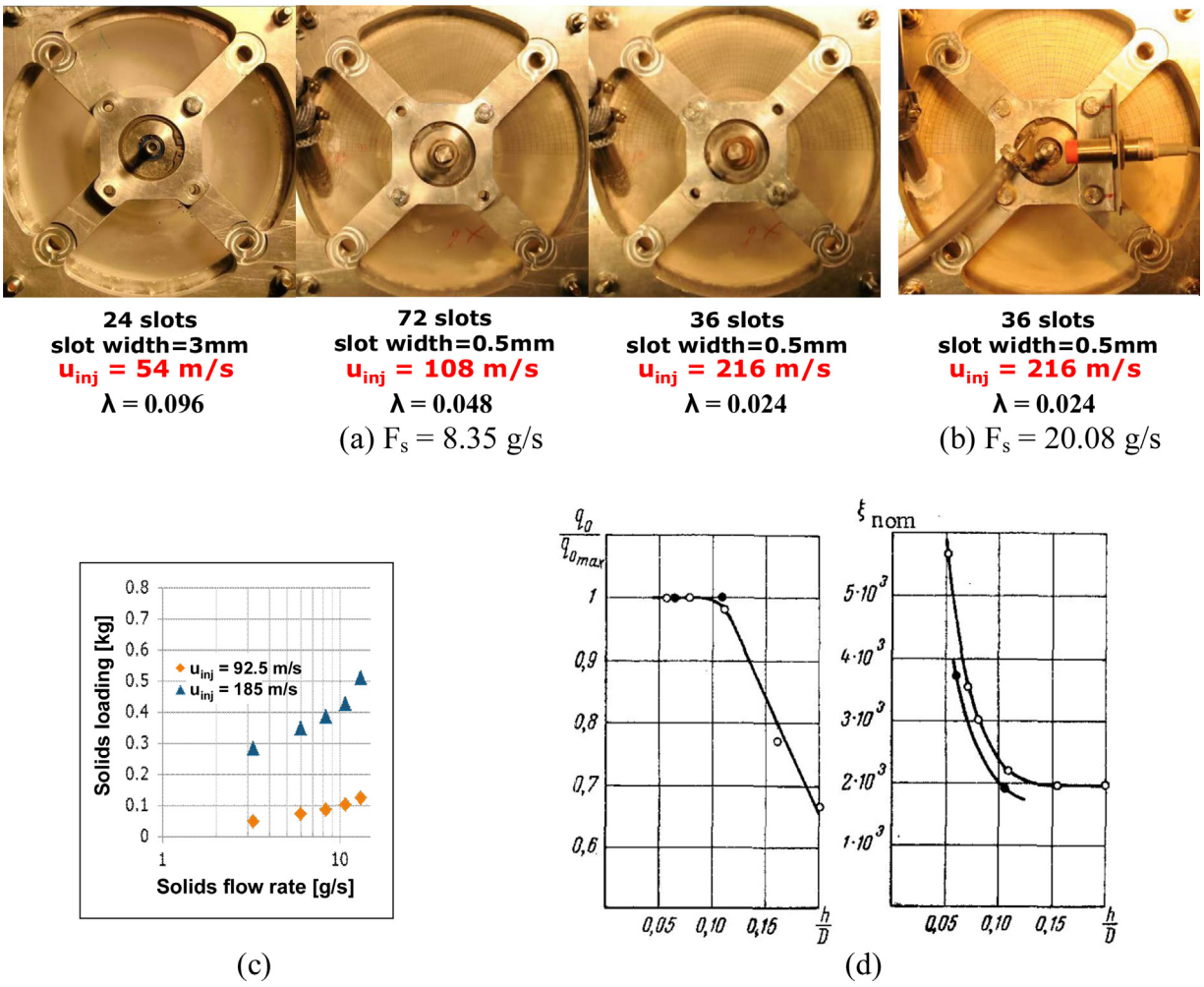

Fig. 14. Influence of λ and the resulting gas injection velocity on the solids loading in a vortex chamber for given gas and solids feeding rates. (a–c) Continuous operation feeding 85 μm FCC catalyst at (a) 8.35 g/s and (b) 20.08 g/s. (c) Solids loading versus solids feeding rate for a given gas flow rate, but different gas injection velocities. Other vortex chamber characteristics and operating conditions as in Fig. 13. (From Ref. [63]). (d) Relative solids retention capacity (zero solids feeding rate) (left) and nominal resistance coefficient (right) as a function of $\pi \times \lambda$ for vortex chambers with D = ○ 12 cm or ● 44 cm and with L/D = 0.29 and D_c/D = 0.25 when feeding Geldart B- or D-type particles (not specified). (From Ref. [43]).

particles (Fig. 11). It is important to notice that an axially non-uniform flow pattern is already observed in the absence of particles. In fact, with the type of particles used by Volchkov et al. [68], the axial uniformity in the vortex chamber is improved by the presence of a particle bed. Still, the reduction of the centrifugal force near the end walls can lead to a lack of cyclostrophic balance and the generation of a secondary flow of particles along the end walls, towards the axis [40]. Observations with smaller particles showed this phenomenon to grow in importance and to be at the origin of excessive particle losses via the chimney. Section 4 deals with the optimization of the vortex chamber design to reduce the latter. Axial non-uniformity intensifies axial motion in the vortex chamber (e.g., [49]). The latter can be significant and eventually used for multi-zone operation and extensions of the concept – see Section 6.

Finally, in many applications, the particles used are poly-disperse in nature. Segregation can then occur inside the vortex chamber. Use can be made of this phenomenon, e.g., to separate grain particles and impurities such as seeds when carrying out grain cleaning in vortex chambers [69]. A poly-disperse solid phase can also result from attrition due to shear in the rotating particle bed in the static vortex chamber. Not many data on shear in rotating fluidized beds in vortex chambers are reported in the literature. De Wilde [19] reported minimal attrition when fluidizing polyethylene particles. With kitchen salt, on the other hand, the protective coating was observed to partially come off, forming a very fine powder that was entrained by the gas into the chimney.

3.7. Rotating fluidized beds in vortex chambers versus conventional fluidized beds

Following the discussion on the hydrodynamic characteristics of rotating fluidized beds in vortex chambers, their differences, advantages and disadvantages with respect to conventional fluidized beds can be summarized. A key difference is that in conventional fluidized beds, the bed is fluidized against earth gravity which is a constant, that is, does not vary with the gas flow rate. Fluidized beds in vortex chambers are operated high-G and the G-force depends on the gas flow rate, the particle bed rotational motion being driven by the tangential injection of the process gas. As a result, fluidized beds in vortex chambers offer an increased flexibility with respect to the gas flow rate but need to be carefully designed to achieve the balance between the centrifugal and radial gas–solid drag forces required to avoid entrainment of particles into the chimney and to build up a dense and uniform bed. The bed does not have to be radially fluidized and the gas and solids fluxes can be controlled independently and in a relatively wide

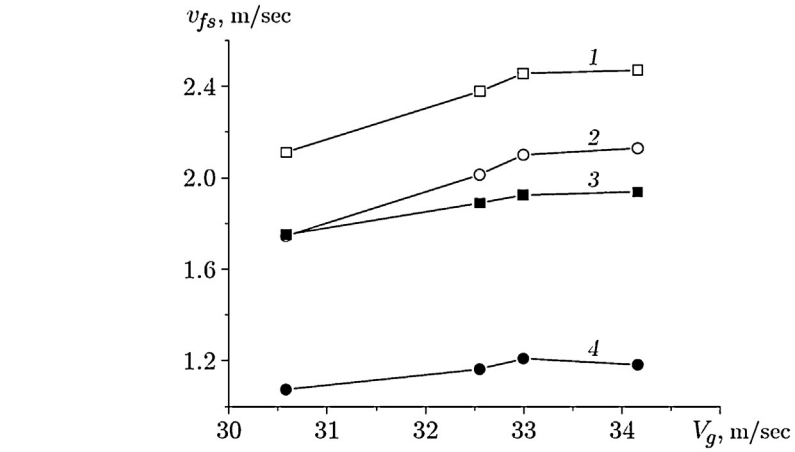

(a)

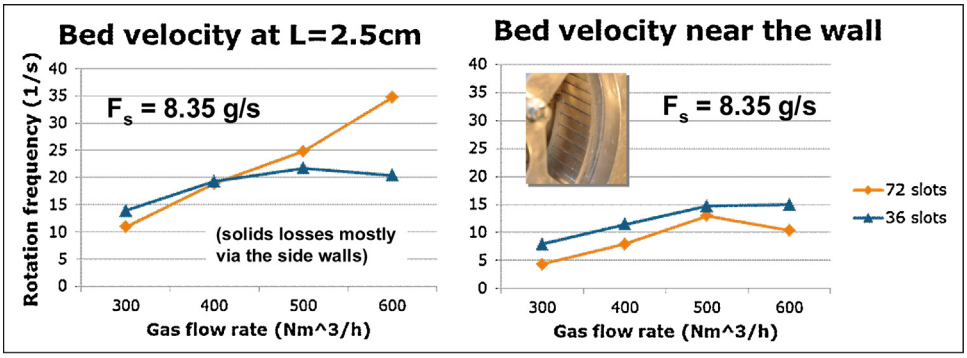

(b)

Fig. 15. (a) Average tangential velocity of the particle bed versus mean gas inlet velocity. (1) Axial center of the upper cylindrical vortex chamber; (3) end wall of the upper cylindrical vortex chamber (2 and 4). Similar in a lower conical vortex chamber – see Fig. 36. (From Ref. [28]). (b) Particle bed rotation frequency versus gas flow rate using two different gas inlet designs (36 and 72 mm × 0.5 mm gas inlet slots) to fluidize 85 μm FCC catalyst in a vortex chamber. Comparison of the rotation velocity near the end wall (right) and in the axial center of the bed (left) to detect channeling. Other vortex chamber characteristics and operating conditions as in Fig. 13. (From Ref. [63]).

range. Because the gas flow rate affects both the centrifugal force and the radial gas–solid drag force, a minimum fluidization velocity or a terminal velocity of the particles in the radial direction cannot be really defined. A minimum gas flow rate is, however, required to achieve high-G operation.

High-G operation allows operation under conditions that cannot be achieved in conventional fluidized beds. The gas–solid slip velocities can be significantly higher than in conventional fluidized beds and dense operation at these high gas–solid slip velocities is possible. Furthermore, bubbling can be suppressed and more uniform particle beds obtained. The cylindrical shape of rotating fluidized beds and high-G operation allow particle bed width-to-height ratios much higher than in conventional fluidized beds, i.e., thin beds. In combination with comparable or higher gas–solid slip velocities, this results in smaller, sometimes extremely small, gas–solid contact times. This can be compensated for by the increased bed density and improved bed uniformity, but the gas usage efficiency or conversion is nevertheless to be carefully evaluated. When carrying out heterogeneous catalytic reactions, the use of a more active catalyst or operation at higher temperature can be considered to allow taking fully advantage of the intensification of interfacial mass, heat and momentum transfer. An example is given in Section 5.

The intensification of interfacial momentum transfer by high-G fluidization in vortex chambers allows fluidizing particles that cannot be properly fluidized in conventional fluidized beds, e.g., cohesive powders, or the introduction of a dispersed liquid phase in relatively high concentrations. An application will be discussed in Section 5. High gas injection velocities are then required resulting in relatively high pressure drops over the gas inlet slots. Finally, even though fluidized beds in vortex chambers allow significant process intensification and novel applications, a major barrier for their application is the difference with conventional fluidized beds, both in hydrodynamic behavior and design. This

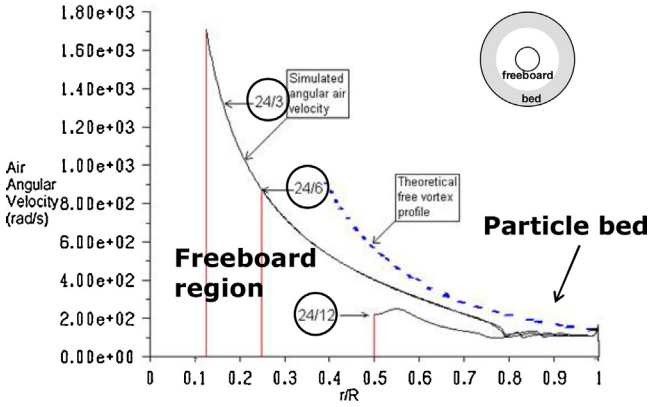

Fig. 16. Influence of the chimney diameter on the angular velocity (radial profiles shown). CFD simulations of the fluidization of 60 μm FCC catalyst in a 24 cm diameter vortex chamber with three different chimney diameters: 3, 6 and 12 cm. Comparison at equal gas flow rate and solids loading. (From Ref. [64]).

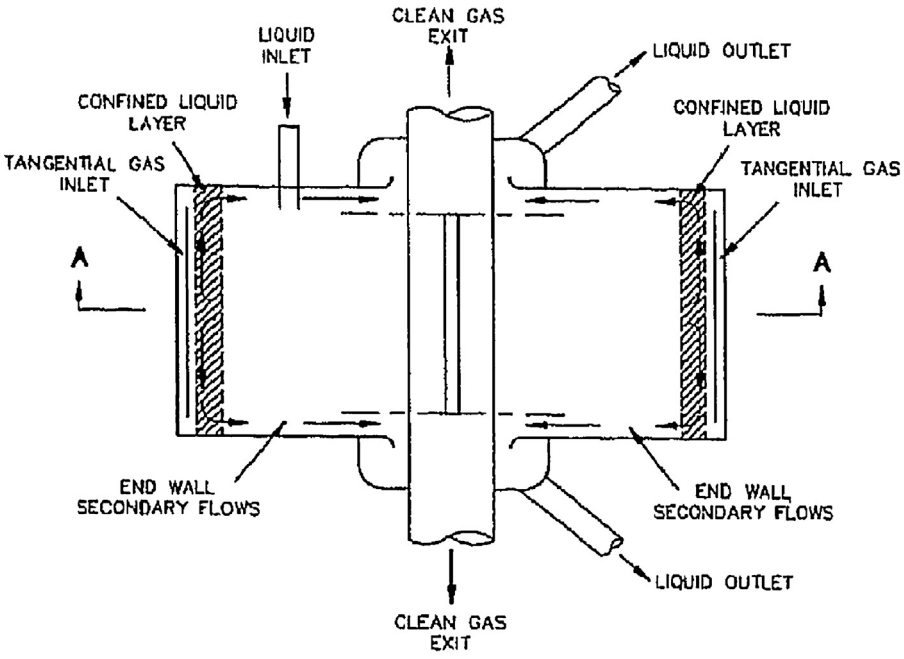

Fig. 17. Dual-chimney design for removal of the heavy (in this case liquid) phase with a symmetric cyclone flow double exit tube with a guide slot for the gas phase. (From Ref. [48]).

means that with given types of particles, you have to account for attrition because of the high shear in the rotating particle bed.

4. Design of vortex type fluidization chambers

In Section 3, the wide variety of flow patterns that can be obtained when fluidizing particles in a vortex chamber was described and the influence of the operating conditions discussed. It was demonstrated that obtaining a dense and uniform particle bed is not obvious. Furthermore, particle losses via the chimney can be pronounced, making an independent control of the gas and solid phase residence times in the vortex chamber challenging. As briefly explained in Section 2, the gas inlet slot design allows modifying the ratio of the radial gas-solid drag force and the counteracting centrifugal force. The flow pattern in the particle bed freeboard region was also shown to have an important impact inside the particle bed. The chimney design has to account for that. Finally, when aiming at continuous operation, the solids feeding and removal system has to be carefully designed to guarantee minimal disturbance of the bed. An overview of the vortex chamber design parameters and operating conditions used in experimental and pilot-scale studies of gas-solid fluidized beds in vortex chambers is given in Table 1. Vortex chambers with diameters ranging from 12 to 82 cm and lengths ranging from 2.4 to 13.5 cm were studied. Reported gas flow rates are in the range 0.01–1.0 m^3/s. As explained in the next section, high-G operation at acceptable gas flow rates, as such allowing sufficient solids retention, can be achieved by injecting the gas at high velocity.

The dimensioning of a vortex chamber is complex. Kochetov et al. [43] report a maximum vortex chamber length of half the vortex chamber diameter ($L < 0.5D$) and optimum chimney diameters between 0.3 and 0.5 times the vortex chamber diameter ($0.3D < D_c < 0.5D$) and chimney entry lengths between 0.1 and 0.2 times the vortex chamber length ($0.1\,L < L_c < 0.2\,L$). Only relatively large Geldart B- and D-type particles were, however, tested, the gas inlet slots were not always uniformly distributed along the circumference and operation was not always high-G. Because of the complex flow pattern in rotating fluidized beds in vortex chambers and the limited amount of data available in the literature, generalization is challenging and a fundamental approach for design and scale-up is necessary. CFD simulations are required, in particular to determine the particle bed rotation speed resulting from the gas injection. Some CFD results will be presented later in this review.

4.1. Gas inlet design

The number of gas inlet slots, n, their individual width, s, and the gas injection angle are critical parameters of the gas inlet design. The influence of the gas injection angle has not been studied so far. This influence can be complex, the gas being immediately deflected upon contact with the particle bed. Most papers consider tangential gas injection. Whereas the number of gas inlet slots has to be sufficiently high to ensure a tangentially uniform gas and solids distribution, the fraction of the chamber circumference taken by gas inlet slots, $\lambda = n \times s/(\pi \times D)$, determines the gas injection velocity for a given gas flow rate and as such the ratio of the radial gas–solid drag force and centrifugal force generated in a vortex chamber. A sufficiently high gas injection velocity is required to allow the generation of a dense rotating fluidized bed and to ensure an axially uniform gas and solids distribution.

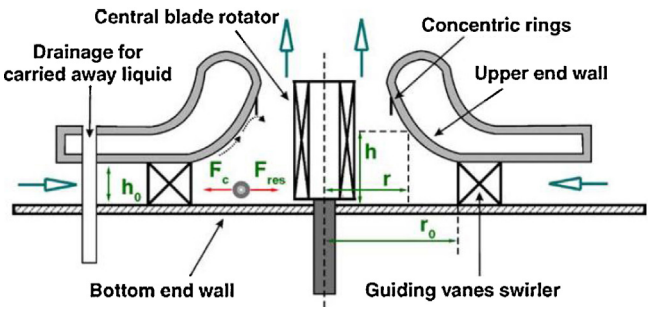

Fig. 18. Profiled end wall-chimney with concentric ring. (From Ref. [46]).

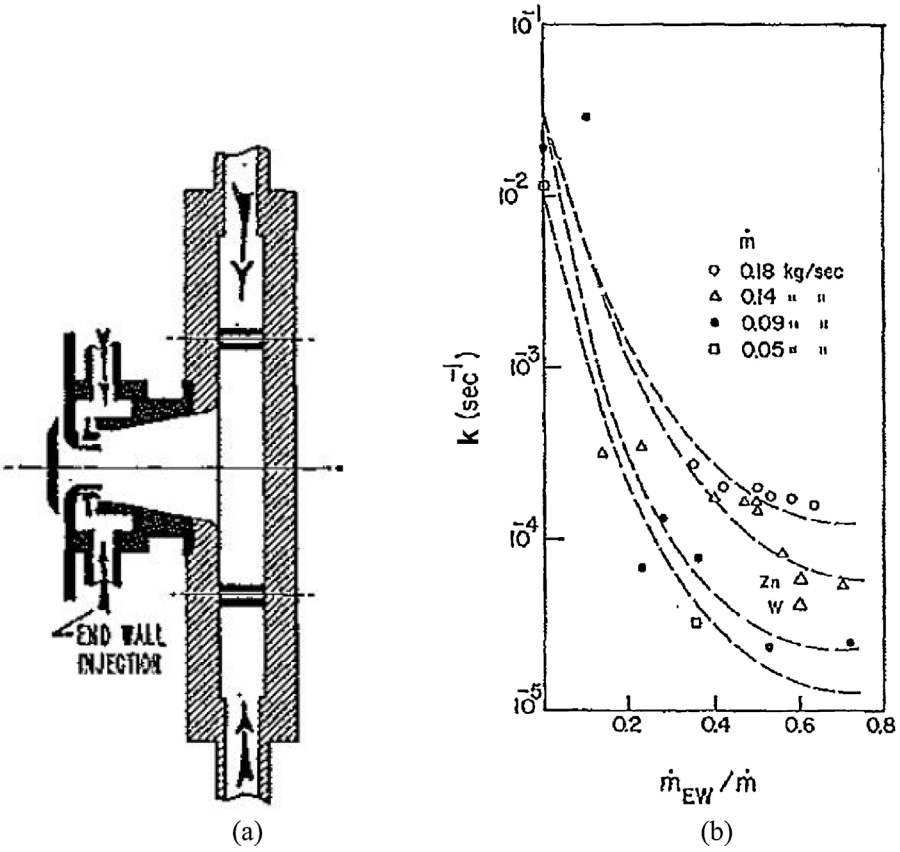

Fig. 19. Vortex chamber with a vortex finder type chimney equipped with secondary gas injection using nozzles positioned concentric to the central gas outlet at the end of a tapered annex. (a) Schematic representation; (b) rate coefficient for particle losses via the gas outlet (chimney) as a function of the normalized secondary gas flow rate for different total gas flow rates. $\dot{m}_{EW}$: secondary (End Wall) gas flow rate; $\dot{m}$: total gas flow rate. (Adapted from Ref. [4]).

Fig. 12(b) illustrates the tangentially strongly non-uniform particle bed obtained when using a single gas inlet slot [44]. To study the effect of a more uniform gas distribution, Kochetov et al. [43] tested vortex chambers of given λ with a single, 5 non-uniformly and 6 uniformly distributed gas inlet slot(s). Fig. 12(c) shows measurements of the solids retention capacity (zero solids feeding rate) of the vortex chambers with the different gas inlet designs as a function of the gas flow rate. In the gas flow rate range studied, gravity is, however, seen to play an important role, that is, operation was not truly high-G. This was also the motivation for testing and recommending a configuration with 5 gas inlet slots positioned in the lower part of the vortex chamber. As long as gravity plays an important role, the retention capacity is seen to increase with increasing gas flow rate. Focusing on the highest gas flow rates, it is seen that, for given λ, increasing the number of gas inlet slots allows increasing the retention capacity. Kochetov et al. [43] chose the number of gas inlet slots for a vortex chamber with given λ such that the width of each slot was commensurate with the bed height. As already clear from Fig. 2 and discussed in more detail hereafter, for a vortex chamber of given λ, the latter depends strongly on the type of particles fluidized. Kochetov et al. [43] recommend 1–3 gas inlet slots for coarsely dispersed particles and 3–5 for finely dispersed. Based on a theoretical analysis on a vortex chamber with given λ and assuming axisymmetrical radial outflow with at least 4 gas inlet slots, Sazhin et al. [55] demonstrated an increase of the solids retention capacity when increasing the number of gas inlet slots up to a given value. For the vortex chamber dimensions and operating conditions considered (D = 0.25 m, L = 0.05 m, λ = 0.025, F_g = 100 m^3/h, ρ_s = 1000 kg/m^3, d_p = 1 mm, 500 μm and 100 μm), a significant increase of the solids retention capacity is predicted when increasing the number of gas inlet slots from 1 to 2 and further to 4. Using more than 4 gas inlet slots had only a minor effect on the solids retention capacity. CFD simulations by De Wilde et al. [21] show axisymmetry with 4 gas inlet slots can, however, be questioned. Volchkov et al. [68] suggest that at least 20 gas inlet slots are required to optimize the particle bed uniformity and maximize the particle bed circulation rate for given gas flow rate and λ. Trujillo and De Wilde [63] carried out an experimental study with different types of particles and vortex chambers with 24, 36 and 72 gas inlet slots and given λ. The data confirm improved bed uniformity and increased bed rotation speed with increasing number of gas inlet slots, at least up to a certain number. The optimal number depends on the type of particles fluidized and in general increases with decreasing particle size and density.

The optimal fraction of the chamber circumference taken by gas inlet slots, λ, also depends on the type of particles fluidized. This is illustrated in Fig. 13, showing the performance of a vortex chamber of given λ when fluidizing different types of particles. Fig. 13(a) focuses on the solids retention capacity of different fractions of polystyrene in a vortex chamber with λ = 0.02 [44]. At sufficiently high gas flow rates, a drastic decrease of the retention capacity with decreasing particle size was observed. Fig. 13(b–d) focuses on continuous solids feeding using a vortex chamber with relatively large λ = 0.096 and given gas and solids feeding rates [63]. The influence of the particle characteristics was confirmed. In particular, no dense and relatively uniform rotating particle bed of 70–85 μm FCC catalyst powder could be obtained in the vortex chamber with λ = 0.096. Kochetov et al. [43] carried out experiments with vortex chambers with λ between 0.016 and 0.064 and relatively large Geldart B- and D-type particles, i.e., various fractions of MSN styrene copolymer, quartz sand, poppy seeds and

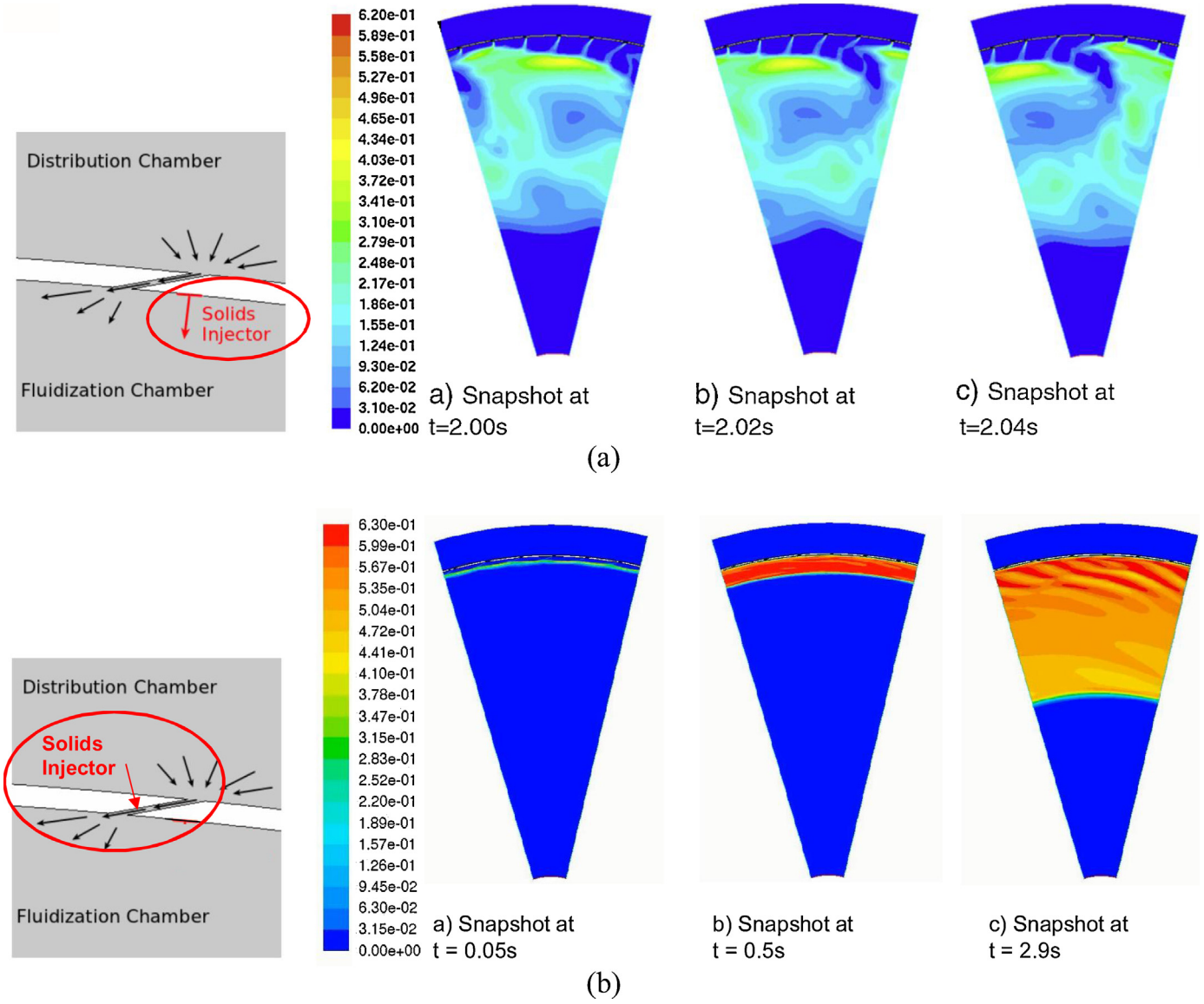

Fig. 20. CFD simulation of the gas–solid flow pattern in a vortex chamber when feeding 80 μm FCC catalyst. Time sequence of the solids volume fraction profile in a vortex chamber with $D = 1.2$ m, $n = 72$, $s = 0.5$ mm, $\lambda = 0.0095$. (a) 72 radial solids inlet slots (from Ref. [65]; (b) solids injection via the gas inlet slots, perpendicular to the gas flow. (Videos can be seen at http://www.uclouvain.be/en-438722.html).

millet. Optimal values of λ between 0.025 and 0.038 were experimentally found, but as mentioned above, both uniformly and non-uniformly distributed gas inlet slots were considered and operation was not always high-G. In later work on the drying of MSN copolymer, sulfanilamide, melalite, and 5 different fractions of polystyrene (d_p: 0.25–0.5 mm, 0.5–1 mm, 1.2–1.5 mm, 1.5–2 mm, 2–2.5 mm) [44], similar chambers and operating conditions were used, but a lower value of $\lambda = 0.02$ was focused on for scale-up studies. Volchkov et al. [68] reported proper functioning of vortex chambers with relatively large λ ($0.05 \leq \lambda \leq 0.1$) with relatively large particles only (sand, corn, wheat grain, and plastic particles with $d_p = 2$–8 mm). Experiments with fine, but high density powders were carried out by Anderson et al. [4], using a vortex chamber with 12 gas inlet slots, only 0.3 mm wide each, resulting in a much smaller λ of 0.00376. A picture of a rotating fluidized bed of fine talc powder ($d_p = 20$ μm, $\rho_s = 2700$ kg/m^3) is shown in Fig. 10. Experiments with higher density tungsten ($d_p = 12$ μm, $\rho_s = 19100$ kg/m^3) and zinc ($d_p = 10$ μm, $\rho_s = 7000$ kg/m^3) powders were also carried out. Anderson et al. [4] reported little indication of bubbling in their experiments. Experimental results by De Wilde and de Broqueville [20,23] confirm the suppression of bubbling when operating high-G at sufficiently high solids loading. The latter is facilitated by correctly choosing λ.

De Wilde et al. [25] derived a theoretical criterium to calculate the maximum slot size as a function of the particle characteristics. It confirms that the maximum λ decreases with decreasing particle size and density. This implies that extremely small slot widths are required to generate a rotating fluidized bed of fine powder, like FCC catalyst, in a vortex chamber. The theoretical criterium is based on the necessary balance between the centrifugal force and the radial gas-solid drag force. Whereas the latter is determined by the gas mass flow rate fed ($\sim \rho\, u_{inj}$), the former depends on the amount of tangential momentum injected with the gas ($\sim \rho\, u^2_{inj}$). Hence, for a given gas mass flow rate, the amount of tangential momentum injected can be varied by changing u_{inj}, i.e., λ. Decreasing λ comes at the cost of an increased pressure drop over the gas inlet slots.

Fig. 14(a–c) illustrates the effect of λ when fluidizing 70 μm (Geldart A-type) FCC catalyst in a vortex chamber at given gas and

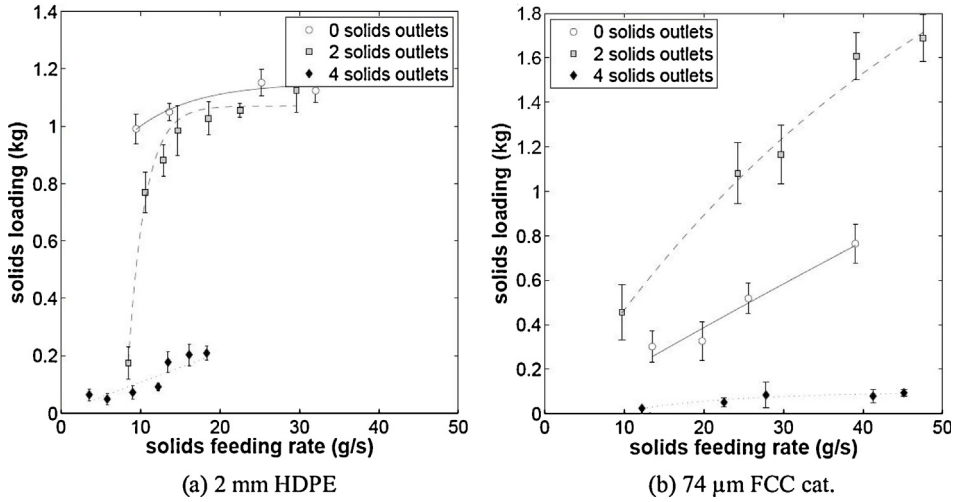

Fig. 21. Influence of the free vortex type flow pattern in the particle bed freeboard region on the solids loading in the vortex chamber for given solids feeding rate. Solids content in the freeboard region affects the flow pattern and can be altered by means of separate solids outlets. Fluidization of (a) 2 mm HDPE polymer pellets and (b) 74 μm FCC catalyst in a vortex chamber of given design with $D = 24$ cm, $L = 5$ cm, $n = 36$, $s = 0.2$ mm, $\lambda = 0.0095$ and operating at a total gas flow rate of 350 m^3/h and a solids loading of 0–1.2/1.8 kg.

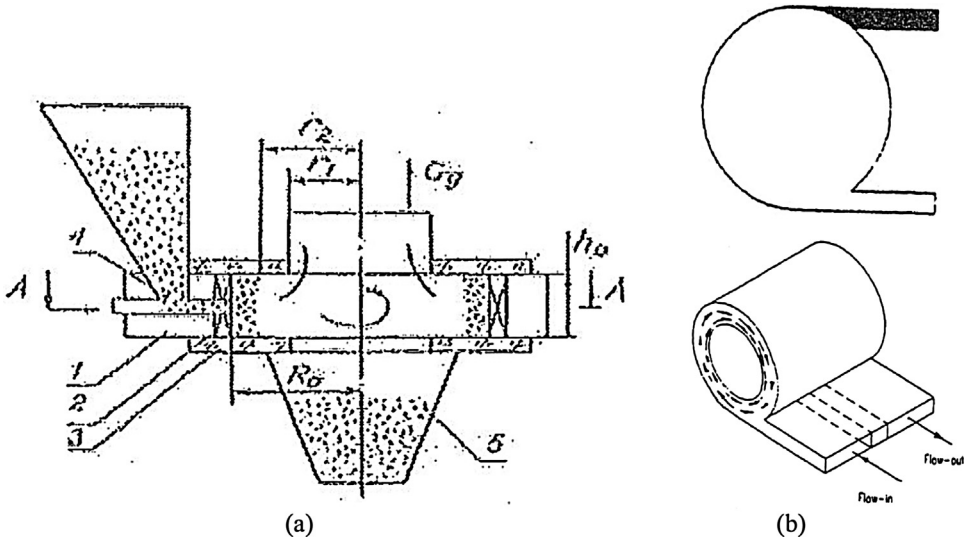

Fig. 22. (a) Vortex chamber with a cyclone type solids recovery system. (1) Gas distribution chamber (helix); (2) vortex chamber; (3) end walls; (4) solids feeder; (5) hopper. (From Ref. [68]). (b) Possible configurations for combining in- and outflow via slots in the outer cylindrical wall of the vortex chamber. (From Ref. [40]).

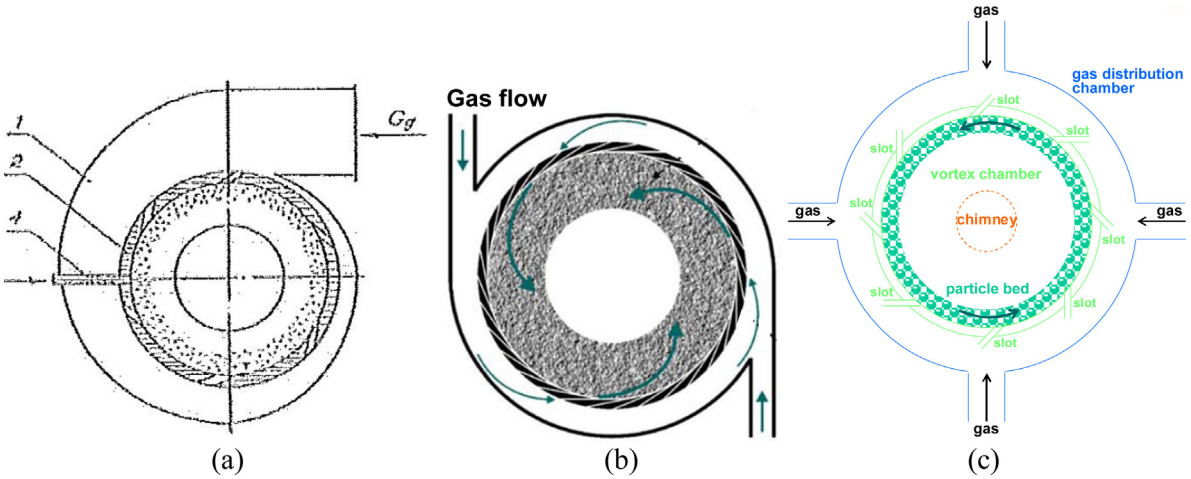

Fig. 23. Possible gas distribution chamber designs. (a) Helix type. (From Ref. [68]); (b) tangentially fed. (Adapted from Ref. [46]); (c) radially fed.

Table 2
2D CFD study of interfacial heat transfer in a conventional fluidized bed and in a rotating fluidized bed in a vortex chamber: Chamber characteristics and operating conditions. (From Ref. [16]).

	Conventional fluidized bed	Rotating fluidized bed in a static geometry
Gas distribution chamber	/	Outer diameter (m): 54×10^{-2} Number of gas inlets: 12 Gas inlet width (m): 3.5×10^{-2}
Fluidization chamber	Width (m): 15×10^{-2} Height (m): 50×10^{-2} Number of gas inlets: 7 Gas inlet width (m): 2×10^{-3}	Outer diameter (m): 36×10^{-2} Number of tangential gas inlet slots: 24 Gas inlet slot width (m): 2.3×10^{-3} Number of solids inlets: 24 Solids inlet slot width (m): 5×10^{-3}
Chimney	/	Diameter (m): $12 - 13 \times 10^{-2}$ Number of outlet slots: 1 Outlet slot width (m): 8×10^{-2}
Solid particles	Diameter (m): 700×10^{-6} Density (kg/m^3): 2500 Restitution coefficient for particle–particle collisions (e): 0.9 Specularity coefficient for particle-wall collisions (ϕ): 0.2 Initial temperature (K): 300 Mass in the fluidization chamber (kg/m$_{\text{length fluid.chamber}}$): 33.75	Mass fed* to the fluidization chamber (kg/m$_{\text{length fluid.chamber}}$): 33.75 *Fed during first 5.63 s of the simulation
Fluidization gas	Flow rate (m^3/(h m$_{\text{length fluid.chamber}}$)): (a) 195 (b) 540 (c) 1080 Temperature (K): 300 → 400 at time t_0	Flow rate (m^3/(h m$_{\text{length fluid.chamber}}$)): (a) 29 800 (b) 59 600

solids feeding rates [63]. Reducing λ clearly increases the centrifugal force (not the radial gas–solid drag force), as such reducing the losses of particles via the chimney, increasing the solids loading (Fig. 14(a and c)) and particle bed density, and improving the particle bed uniformity, i.e., suppressing the formation of meso-scale non-uniformities (bubbles). Similar findings were reported by Ekatpure et al. [29]. In a vortex chamber with $\lambda = 0.127$, a rotating particle bed of relatively large polymer particles ($\rho_s = 950$ kg/m^3, $d_p = 0.9$, 1.6 and 2.4 mm) could be obtained, but not of fine FCC catalyst powder ($\rho_s = 1500$ kg/m^3, $d_p = 70$ μm). The latter required reducing λ to 0.042. Fig. 14(d) shows earlier data by Kochetov et al. [43] with Geldart B- or D-type particles (not specified) and for 12 and 44 cm diameter vortex chambers with a single gas inlet slot. The normalized solids retention capacity and resistance coefficient are shown as a function of $\pi \times \lambda$. The resistance coefficient reflects the system pressure drop. The data confirm that a sufficiently small λ is required, but reducing the value of λ beyond a given value no longer improves the solids retention, while the resistance coefficient keeps increasing. Optimal values of λ between 0.025 and 0.038 were reported for the particles used. The influence of the particle characteristics on the optimal λ was not studied. Kochetov et al. [43] suggest a lower boundary of the slot width commensurate with the bed height which depends on the particle characteristics. Anderson et al. [4], Trujillo and De Wilde [63] and Eliaers et al. [34] found that smaller slots are required with fine particles, but in order to have an optimal exchange of tangential momentum between the gas injected and the particles, the use of a gas inlet slot size smaller than the particle diameter has to be avoided, i.e., $s > d_p$. Hence, a vortex chamber design that works for small particles may not work for large particles and vice versa.

Axial non-uniformity in the rotating particle bed, channeling in extremis, can be detected through differences in the pressure or the rotation speed. Using Laser Doppler Velocimetry (LDV) and a rotating antenna, Dvornikov and Belousov [28] measured significantly lower particle bed rotation speeds near the end walls than in the axial center when drying relatively large particles ($\rho_s = 1420$ kg/m^3, $d_p = 3.5$ mm) in a vortex chamber with $\lambda = 0.1$ (Fig. 15(a)). A similar finding was reported by Trujillo and De Wilde [63] when fluidizing FCC catalyst ($\rho_s = 1500$ kg/m^3, $d_p = 85$ μm) in a vortex chamber with $\lambda = 0.048$ and the axial gradients in the rotation speed were found to increase with increasing gas flow rate (Fig. 15(b)). Reducing λ0.024, as such increasing the pressure drop over the gas inlet slots, allowed improving the axial uniformity in the vortex chamber (Fig. 15(b)). Improved axial uniformity requires a pressure drop over the gas inlet slots that is significant compared to the pressure drop over the bed. As shown in Section 3, the pressure drop over the bed depends on the particle properties, but the relation is complex because the bed is

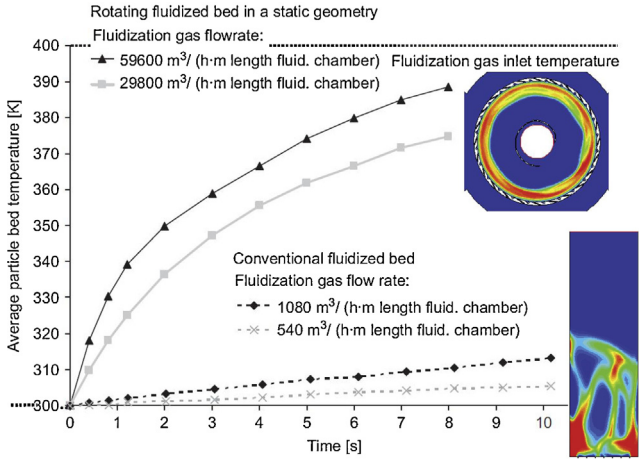

Fig. 24. 2D CFD simulations of the response of the average particle bed temperature to a step change in the gas phase temperature from 300 to 400 K at $t = 0$ s. Comparison of a conventional fluidized bed and a rotating fluidized bed in a vortex chamber. Embedded contour plots of the solids volume fraction (snapshot). Chamber design and operating conditions: see Table 2. (Adapted from Ref. [16]).

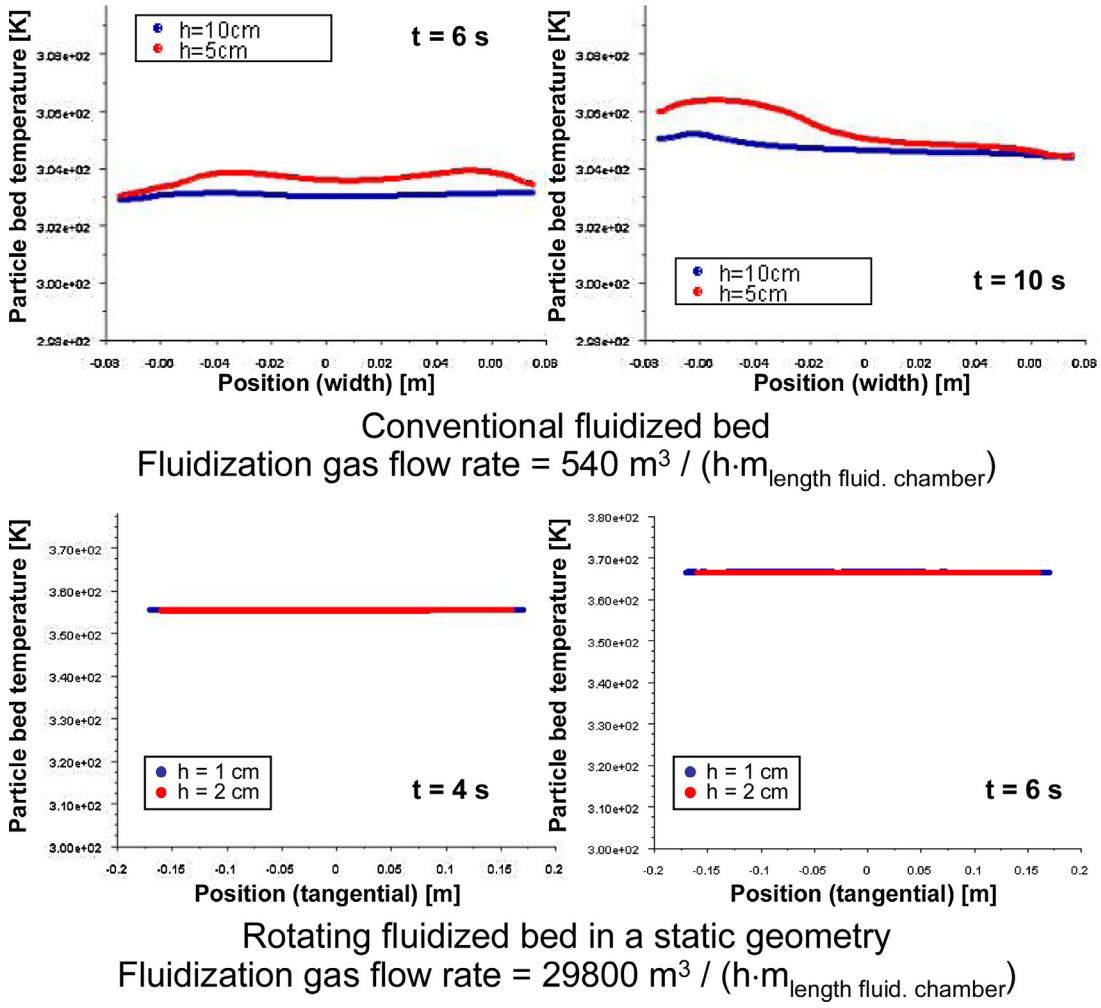

Fig. 25. 2D CFD simulations of the response of the particle bed temperature to a step change in the gas phase temperature from 300 to 400 K at $t = 0$ s. Comparison of the particle bed temperature uniformity in a conventional fluidized bed and in a rotating fluidized bed in a vortex chamber. Chamber design and operating conditions: see Table 2. (Adapted from Ref. [16]).

not necessarily radially fluidized. Note that the risk of axial non-uniformity increases with increasing vortex chamber length. Kochetov et al. [43] report a significant increase of the axial non-uniformity and related axial flows and solids losses via the chimney for lengths more than half the vortex chamber diameter.

4.2. Gas outlet/chimney design

The chimney design affects the rate of solids losses via the chimney. The latter can occur when particles start moving radially inwards, i.e., when the centrifugal force is not sufficiently strong to compensate for the radial gas-solid drag force. Because of friction, the risk of such a lack of cyclostrophic balance is particularly high near the end walls and can generate a significant boundary layer, secondary flow [40]. Loftus et al. [48] proposed to use the secondary flows near the end walls to remove the heavy phase from the vortex chamber using a concentric dual-chimney design as presented in Fig. 17. To reduce the rate of solids losses via the chimney and improve the bed stability and density for given operating conditions, different chimney designs have been tested, but a rigorous comparison of the resulting performance was only made for gas–liquid flows [48]. A cyclone flow exit tube completely inserted into the vortex chamber and equipped with a guide slot is shown in Figs. 1, 2 and 17. A so-called vortex finder, which is essentially an open ended tube, is shown in Figs. 10–14 and 19. To reduce solids losses via the chimney due to secondary flows near

Table 3
Drying of granular materials in a vortex chamber. Vortex chambers as shown in Fig. 12(b) but with multiple gas inlet slots when drying fine particles (5 gas inlet channels in the lower part of the chamber or 6 evenly distributed). (From Ref. [44]).

Material	Output, kg/h	Air flow rate, kg/h	Gas temperature, °C		Moisture content of material, %		Average time material in apparatus, sec
			Initial	Final	Initial	Final	
MSN copolymer	16.0	120	140	90	8.0	0.5	11
Sulfanilamide	18.0	96	180	106	12.0	0.1	23
Melalite	3.6	102	185	130	40.0	1.5	185
Emulsion polystyrene	2.8	50	140	100	27.0	0.60	15

Note: In drying the finely divided materials (polystyrene, sulfanilamide, MSN copolymer) inserts were mounted within the vortex chambers, permitting gas to be supplied through several channels to the rotating annular layer of particles.

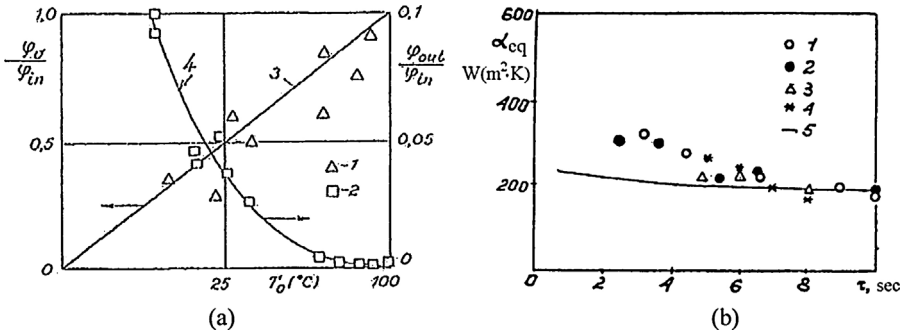

Fig. 26. (a) Fraction of moisture evaporated and evaporation efficiency versus gas temperature during continuous drying of sand (ρ_s = 1900 kg/m^3, d_p = 2 mm) in a vortex chamber of given design with D = 36 cm, L = 6 cm, D_c = 8 cm, n > 20, λ = 0.099 and operating at a solids feeding rate of 10–40 g/s with φ_{in} = 0.15 and a gas flow rate of 50–100 g/s. (From Ref. [68]). (b) Effective heat transfer coefficient for heat transfer between the gas and the grain particles versus the grain heating time. (1) Re = $\rho_g u_{inj} d_p/\mu_g$ = 2600; (2) Re = 1800; (3) Re = 2000; (4) Re = 2300 (industrial test); (5) simulation model for a single particle, Re = 1800, Bi = 1.26. Industrial test with grain flow rate = 30 t/h, grain inlet temperature = 11 °C, grain inlet moisture content = 25%, air flow rate (vortex chamber) = 22.5 t/h, air inlet temperature (vortex chamber) = 206 °C. (From Ref. [69]).

Table 4
Drying chamber characteristics and operating conditions. (From Ref. [33]).

	Conventional fluidized bed	Rotating fluidized bed in a static geometry
Dimensions	D = 0.10 m H = 1.50 m V = 11.8 L	D = 0.43 m D(chimney) = 0.10 m L = 0.05 m V = 6.9 L
Gas distribution	Cone and perforated plate	72, 30° inclined gas inlet slots, 2 mm width each λ = 0.107
Solids feeding	Via side wall at h = 0.05 m	Via end wall
Particle characteristics	Pelletized wood, cylindrically shaped, d_p = 4 mm, h_p = 4 mm	
Operating conditions		
T_{bed}(K)	318.15	
P_{out}(Pa)	101325	
Gas mass flow rate (Nm^3/h)	110	700
Solids mass flow rate ($g_{humid\ biomass}$/s)	1,2,3, 6, 9	3, 6, 9, 12, 15, 18
Solids inlet moisture content (g_{water}/$kg_{dry\ biomass}$)	850	

the end walls, the vortex finder can eventually be inserted over a short length into the vortex chamber or concentric rings can be placed on the end walls at a certain distance from the chimney [43]. Compared to cyclone flow exit tubes with a guide slot, vortex finders are expected to reduce the rate of solids losses via the chimney and to improve the bed stability. A vortex finder is less intrusive and allows a more efficient return of radially entrained particles to the bed by the Coriolis effect–inertia transforming radially inward motion of a rotating particle into tangential and next radially outward motion. The latter requires the particles to follow their trajectory undisturbed and without being lost into the chimney. A particle-free freeboard region in which a free vortex type flow pattern develops (as in Fig. 4) intensifies the Coriolis effect. As such, a free vortex in the freeboard region contributes driving the particle bed rotational motion, together with the tangential injection of the gas through the gas inlet slots. Reducing the chimney diameter increases the time during which the particles are exposed to the Coriolis effect in the freeboard region. The positive effect of the latter on the bed stability and solids retention, as illustrated in Fig. 16 and experimentally confirmed by Loftus et al. [48], comes at the cost of a higher pressure drop over the chimney. A symmetric double chimney design (Fig. 17) allows avoiding a too high pressure drop. The stability of operation with a double chimney is, however, to be studied in more detail. The use of a double chimney will also affect the (effects of) under-pressure typically observed near the central axis of the vortex chamber and in particular the axial motion in the vortex chamber. Data on vortex chambers with a perforated end plate are worth looking at in this context [49]. Using a single vortex finder type chimney and testing

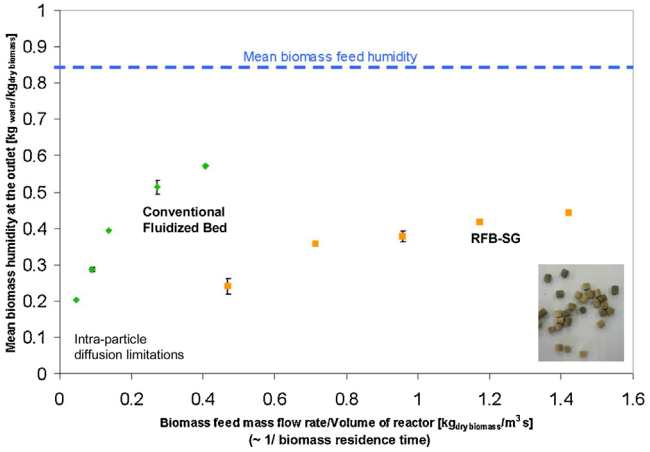

Fig. 27. Mean biomass moisture content at the in- and outlet versus the specific biomass feed rate when drying woody biomass particles in a conventional fluidized bed and in a vortex chamber based high-G dryer (RFB-SG). Drying chamber characteristics and operating conditions: see Table 4. (From Ref. [31]).

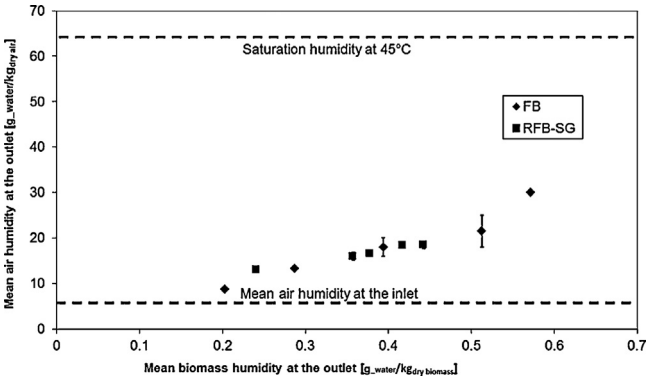

Fig. 28. Mean air humidity at the in- and outlet versus the mean biomass moisture content at the outlet when drying woody biomass particles in a conventional fluidized bed and in a vortex chamber based high-G dryer (RFB-SG). Drying chamber characteristics and operating conditions: see Table 4. (From Ref. [33]). See original figure caption.

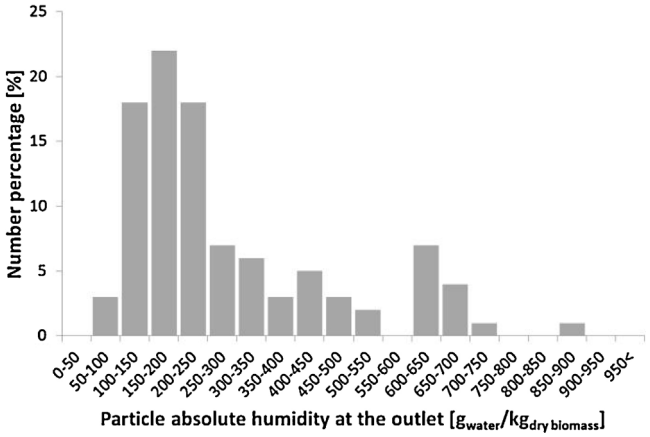

Fig. 29. Drying of granular biomass in a vortex chamber. Particles bypassing the rotating particle bed and going directly from the side solids inlet into the chimney indicated by a bimodal distribution of the outlet biomass moisture content. (From Ref. [33]).

different vortex chamber designs with relatively large Geldart B- and D-type particles, Kochetov et al. [43] reported maximum solids retention with a chimney diameter of 0.3–0.5 times the gas distribution chamber diameter and a chimney entry length between 0.1 and 0.2 times the vortex chamber length. It is expected that with lighter powder, the use of a smaller chimney will be advantageous, although this will increase the hydraulic resistance of the system.

In their experiments with fine powders, Anderson et al. [4] adapted the chimney design to suppress the boundary layer flow at the origin of the major part of the solids losses via the chimney. Additional nozzles for secondary gas injection were positioned concentric with the gas outlet, located centrally at the end of a tapered annex (Fig. 19(a)). Fig. 19(b) shows the positive effect of the secondary gas injection on reducing the rate of solids losses via the chimney. The latter is quantified by means of a rate coefficient, k, that is defined based on the experimental observation that in a radially fluidized rotating fluidized bed the rate of solids losses via the chimney is proportional to the solids loading in the vortex chamber, $-dM/dt \sim k \times M$, leading to an exponential decrease of the solids loading after stopping continuous solids feeding resulting in a solids loading M_0:$M = M_0 \exp[-k \times t]$ [4,24]. The use of secondary gas injection as proposed by Anderson et al. [4] may, however, be undesired in certain applications, e.g., when the process gas is to be converted by the particles or is used to convert the particles.

Balancing the centrifugal force and the radial gas–solid drag force was considered to be essential to avoid solids losses via the chimney and the Coriolis effect was often neglected in the analysis and design of vortex chambers. Because rotating fluidized beds are cylindrical and have a close to solid body type rotational motion when sufficiently dense, the ratio of the radial gas–solid drag force to centrifugal force grows when moving radially inwards, i.e., due to the decreasing circumference. Volchkov et al. [68] and Kuzmin et al. [46] proposed profiling the end wall of the vortex chamber connected to the chimney to compensate for this, allowing balancing the radial gas–solid drag force and the centrifugal force throughout the vortex chamber. Kuzmin et al. [46] theoretically calculated the end wall profile and added a concentric ring to further reduce solids losses via the chimney (Fig. 18). Although a significant and positive influence of profiling the end wall was found by Kuzmin et al. [46], profiling the end wall has the disadvantage of destroying the free vortex in the particle bed freeboard region, critical for maximizing the Coriolis effect that allows reducing solids losses via the chimney.

4.3. Solids inlet design

Solids can be injected via the end walls (side solids inlet) or via the outer cylindrical wall. Remark that for normal operation of a rotating fluidized bed in a vortex chamber and to facilitate uniform operation, the contribution of the solid phase to the amount of tangential momentum injected should be negligible, i.e., the

Table 5
Operating conditions for the low-temperature wet coating of a cohesive powder in a 0.24 m diameter vortex chamber with $\lambda = 0.019$. (From Ref. [34]).

	Operating variable	Unit			
Air	Flow rate	Nm^3/h	250	400	
	Pressure before distributor	mbar	300–370	540–650	
	Inlet temperature	K	328.15	328.15	
Powder	Feed rate	g/s	2	2	
	Density	kg/m^3	260	260	
	Mean particle diameter	μm	69.71	69.71	
Coating solution (aqueous)	Feed rate	g/s	1	1	1.63
	Injection pressure	bar	1.5	1.5	3
	Mean droplet diameter	μm	70	70	60
	Inlet temperature	K	363.15	363.15	363.15
	Fraction coating material w_{cm}	wt.%	50	50	50
	Coating material density	kg/m^3	1340	1340	1340
	Coating time	s	5, 15, 30, 60	3, 5, 15, 30, 60	5

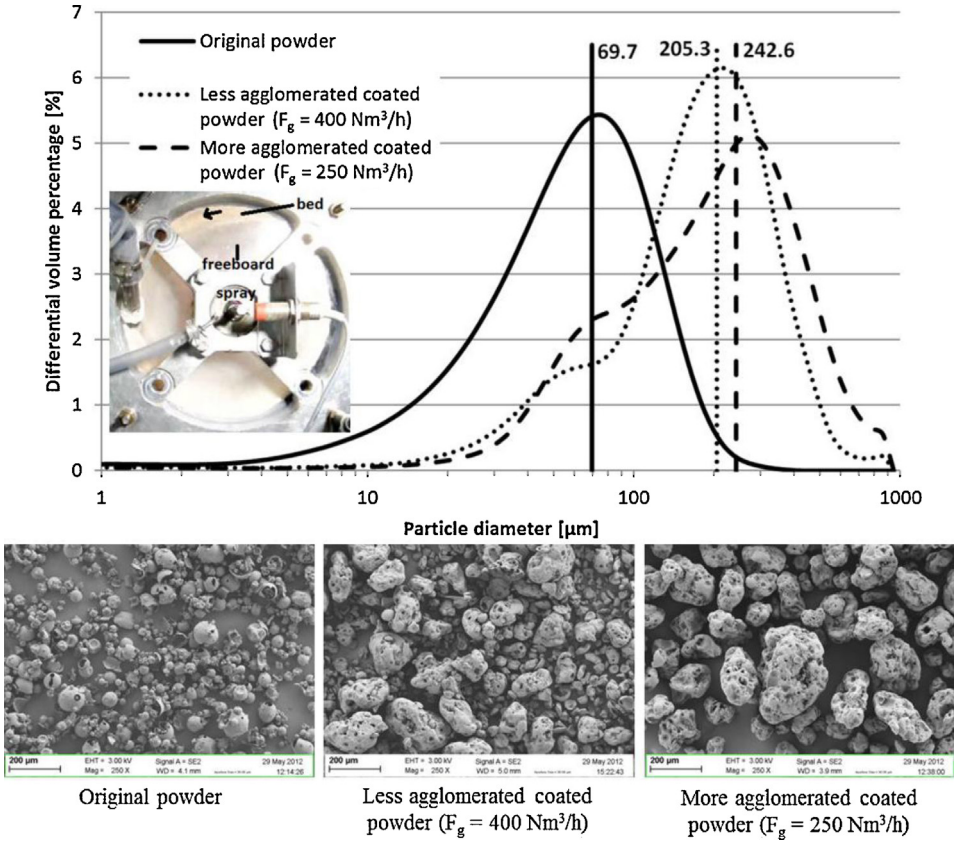

Fig. 30. Particle size distribution and SEM pictures of the uncoated powder and of less and more agglomerated coated powder. Less agglomerated coated powder: air flow rate = 400 Nm^3/h; more agglomerated coated powder: air flow rate = 250 Nm^3/h. Other operating conditions: core material feed rate = 2 g/s, coating solution feed rate = 1 g/s, coating time = 5 s. Picture of a rotating particle bed of the cohesive (Geldart C-type) powder in the 0.24 m diameter vortex chamber with $\lambda = 0.019$ also shown. (From Ref. [34]).

particle bed rotational motion should be driven by the gas phase. In case of a side solids inlet, a tube is typically pierced through the end wall(s). The use of a peripheral slot was also considered [28]. De Wilde and de Broqueville [20,22,24], Trujillo and De Wilde [63], Eliaers and De Wilde [31–33] and Eliaers et al. [34] showed a side solids inlet tube to function properly with Geldart A,B,C and D-type particles in a wide solids feeding rate range. Too high solids feeding rates may, however, disturb the hydrodynamics of the rotating particle bed. Furthermore, the residence time of the particles in the vortex chamber should be sufficiently high for the particles to form a rotating fluidized bed, i.e., to complete a couple of rotations in the vortex chamber. The radial position of the side solids inlet has been shown to have an important effect on the solids losses via the chimney. In order to avoid too much influence on the particle bed hydrodynamics, solids should be fed in the particle bed freeboard region. If positioned too closely to the chimney, however, direct entrainment of the particles fed into the chimney can occur [31,33]. When the solids are injected via the outer cylindrical wall and injection of tangential momentum with the solids is to be avoided, radial injection via separate solids inlet slots can be considered (Fig. 20(a)). CFD simulations showed, however, that the latter is detrimental for the particle bed stability. Alternatively, the solids can be fed into the gas inlet slots, after which they are entrained by the gas into the vortex chamber (Fig. 20(b)). In such case, the inlet slots have to be sufficiently wide to avoid blockage by the particles. If extremely small gas inlet slots are required (see Section 4.1), solids feeding via the gas inlet slots becomes challenging. Both CFD simulations and experimental tests showed an improved bed stability compared to when solids are injected radially through the cylindrical wall [65]. In tests with relatively large particles (sand, corn, wheat grain, and plastic particles with d_p = 2–8 mm), Volchkov et al. [68] fed the solids via the outer cylindrical wall of the vortex chamber, but in the axial center only. It is not clear if separate gas and solids inlet slots were used.

4.4. Solids outlet design

The solids outlet is evidently crucial for processes requiring continuous solids feeding and removal and was found to have a significant effect on the particle bed stability and the solids loading that can be built up in the vortex chamber for a given solids feeding rate [20]. As with the solids feeding, the end walls or the outer

Table 6
Composition of the uncoated powder and of less and more agglomerated coated powder and data of an active component (a.c.) release test. Less agglomerated coated powder: air flow rate = 400 Nm^3/h; more agglomerated coated powder: air flow rate = 250 Nm^3/h. Other operating conditions: core material feed rate = 2 g/s, coating solution feed rate = 1 g/s, coating time = 5 s. (From Ref. [34]).

Powder	d_p (µm)	ρ_s (kg/m³)	Core material (wt.%)	Coating ($g_{coating}/g_{core}$)	A.c. release (%)	Reduction of a.c. release
Uncoated powder	69.7	260	100	–	60	–
Less agglomerated coated powder (Fg = 400 Nm^3/h)	205.3	657	63.23	0.58	24	60%
More agglomerated coated powder (Fg = 250 Nm^3/h)	242.6	660	62.96	0.59	24	60%

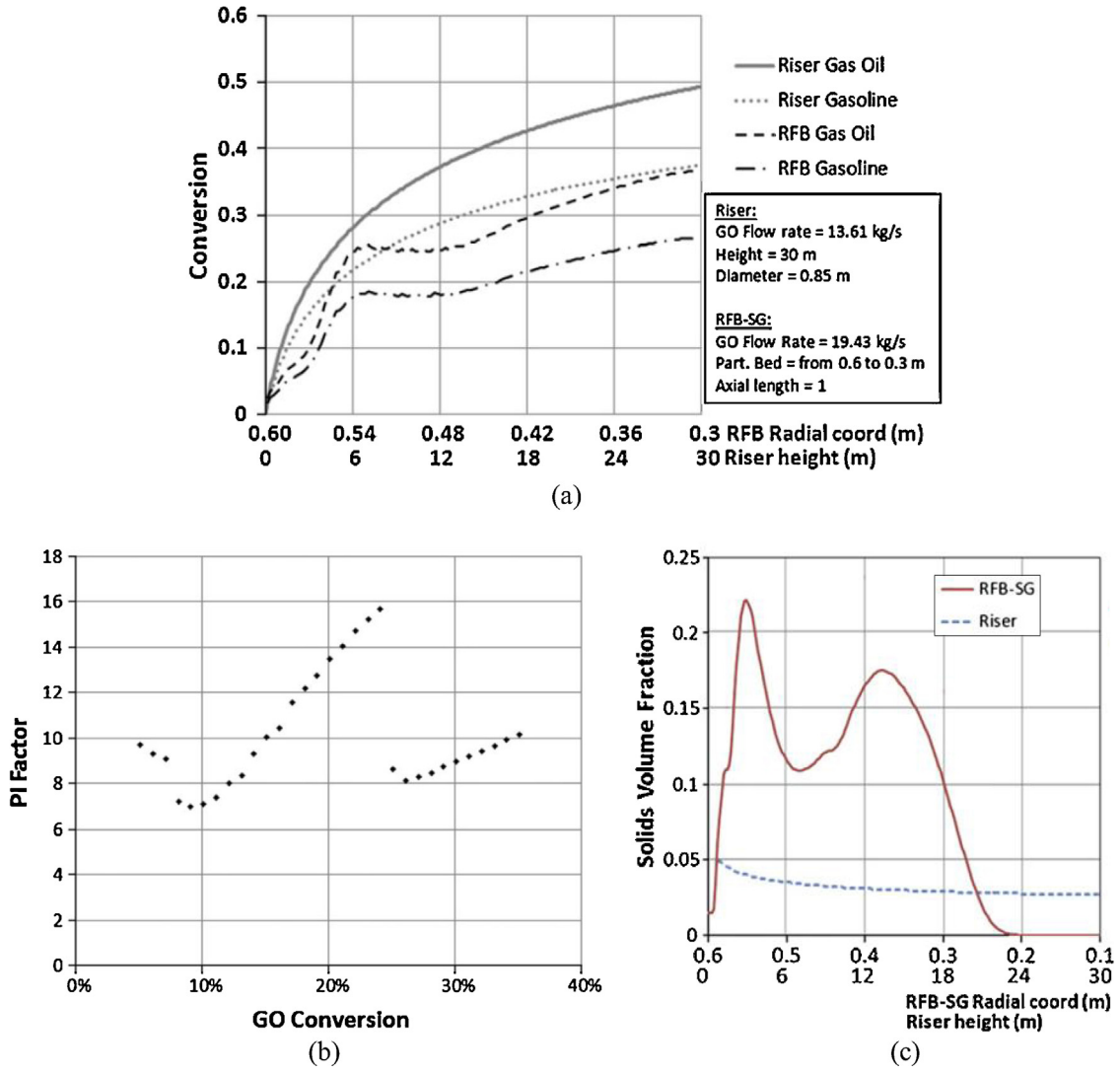

Fig. 31. Numerical comparison of the performance of vortex chamber based (RFB-SG) and reference riser technology in the fluid catalytic cracking of gas oil. (a) Gas oil (GO) conversion and conversion into gasoline versus the distance in the reactor particle bed. (b) Process Intensification (PI) factor as a function of the GO conversion. (c) Radial/axial profiles of the solids volume fraction in the RFB-SG/riser reactor. Riser simulated by means of a 1D model, the vortex chamber by means of a 2D periodic domain CFD model. Reactor characteristics and operating conditions: for the vortex chamber: see Table 7; for the riser reactor: given in the figure (a). (Adapted from Ref. [65]).

cylindrical wall can be used to remove the solids separately from the gas. If no solids outlet is foreseen, the solids will leave with the gas via the chimney when stationary operation is reached and separation from the gas is to be carried out downstream from the vortex chamber.

Continuous feeding and removal of 3 mm HDPE polymer pellets via tubes pierced through the end walls was demonstrated by De Wilde and de Broqueville [20] (a video can be seen at http://www.uclouvain.be/en-438722.html). In their experiments, no solids losses via the chimney were observed and the particle bed freeboard region was particle free. With lighter 1G-Geldart A-, B- and C-type particles, solids losses via the chimney are typically more pronounced [20,63]. A separate solids outlets then allows reducing the solids content in the particle bed freeboard region, facilitating the generation of a free vortex type flow pattern in this region. The latter maximizes the Coriolis effect returning particles from the freeboard region to the bed and stabilizes the bed (see also Section 4.2). Fig. 21 shows the solids loading of (a) 2 mm HDPE particles and (b) 74 μm FCC catalyst powder as a function of the solids feeding rate in a 24 cm diameter vortex chamber with 36 gas inlet slots, 0.2 mm wide each, and a vortex finder type chimney, when using different solids outlet configurations. It is remarkable that with FCC catalyst powder and for given operating conditions, a higher solids loading can be built up when 2 separate side solids outlets are foreseen than with no separate solids outlets, due to a reduction of the solids content in the freeboard region. With more, i.e., 4 solids outlets, the solids leave the vortex chamber too easily and building up a bed becomes again more difficult.

An annular solids outlet slot in one of the end plates was proposed by Dvornikov and Belousov [28] (see Fig. 36(b) discussed later), but used with relatively large particles only (d_p = 3.5 mm, ρ_s = 1420 kg/m^3). In Section 4.2, the importance of boundary layer flows along the end walls was discussed, especially important when fluidizing lighter particles. Loftus et al. [48] designed the solids outlet in the end wall to take advantage of this effect (Fig. 17). Volchkov et al. [68] presented a cyclone type solids outlet (Fig. 22(a)) and used it with different types of relatively large particles (sand, corn, wheat grain and plastic, d_p = 2–8 mm). Goldshtik et al. [40] considered removing the heavy phase via the outer cylindrical wall of the vortex chamber, see Fig. 22(b). The top configuration was found to be much less perturbing for the

Table 7
2D periodic domain CFD simulation of fluid catalytic cracking (FCC) of gas oil in a vortex chamber: reactor characteristics and operating conditions. (Mass flow rates: per m length vortex chamber.) (From Ref. [65]).

Distribution chamber	Gas mass flow rate	8.35	kg/s/m
	Gas inlet density	4.72	kg/m^3
	Gas inlet temperature	775	K
Fluidization chamber	Number of slots	72	–
	Slots width	0.5	mm
	Outer radius	0.6	m
	Inner radius (chimney)	0.1	m
	Particle diameter	80	μm
	Particle density	1500	kg/m^3
	Catalyst mass flow rate	181.44	kg/s/m
	Catalyst volume fraction at the inlets	0.3	–
	Catalyst initial coke content	0.15	wt.%
	Catalyst inlet temperature	775	K
	Feed cat-to-oil ratio	21.75	–

flow in the vortex chamber than the bottom one with a divided channel causing symmetry breaking.

4.5. Other design aspects

The influence of the gas distribution chamber design on the flow pattern in the vortex chamber can be questioned and different designs have been studied (Fig. 23). The helix type gas distribution chamber aims at uniformizing the gas flow rate over the different gas inlet slots of the vortex chamber. Tangentially fed gas distribution chambers aim at already generating a rotational flow in the gas distribution chamber. De Wilde [19] showed that both issues are irrelevant for the flow pattern in the vortex chamber, provided that the pressure drop over the gas inlet slots of the vortex chamber is sufficiently high, that is, λ is sufficiently small.

The vortex chamber itself can be cylindrical, polygonal or complexely shaped. The influence on the crucial transfer of tangential momentum between the injected gas and the particles is important [27]. Friction with the wall in the immediate vicinity of the gas inlet slots is to be avoided. Hence, a polygonal design is usually advantageous. Furthermore, it facilitates the construction of the vortex chamber.

5. Case studies

5.1. Biomass drying

When fluidizing in a high-G field, operation at high gas–solid slip velocities and related coefficients of interfacial mass, heat and momentum transfer is possible. Vortex chambers offer the additional advantage of the flexibility in the gas flow rate and the high specific gas flow rate (m^3 gas/m^3 particle bed) [22,23]. By means of a CFD step response study, de Broqueville and De Wilde [16] illustrated the intensification of interfacial heat transfer in rotating fluidized beds in vortex chambers. Details of the simulations are given in Table 2. Fig. 24 shows the response of the temperature of the particle bed to a step change of the temperature of the fluidization gas for both a conventional fluidized bed and a rotating fluidized bed in a vortex chamber. A much faster response can be generated in the latter. The CFD simulations also demonstrated the improved uniformity of the particle bed temperature in vortex chambers, due to intense mixing at high particle bed rotation speed (Fig. 25).

Application of vortex chamber technology for the drying of granular materials has been considered by different groups. The removal of superficial moisture from several materials listed in Table 3 and from sand was studied by Kochetov et al. [44] and Volchkov et al. [68]. No direct comparison with drying in a conventional fluidized bed was made, but a fast removal of superficial moisture was demonstrated. Focusing on continuous sand drying at relatively mild temperatures, Fig. 26(a) shows the fraction of moisture evaporated and the related evaporation efficiency as a function of the gas feed temperature for the given vortex chamber design and operating conditions [68]. Deep dehydration of sand ($\Delta\varphi$ = 0.15–0.2) can be achieved with particle residence times of only 3–5 s. Aerodynamic blow off of superficial moisture was indicated to contribute significantly to the rapid drying of sand in vortex chambers, in particular at low temperatures, although it is unclear to what extent the liquid droplets blown off evaporate [68].

When drying materials which contain bound and capillary moisture, such as grain, fast initial drying can be achieved in vortex chambers [68,69,31,33]. A decrease from 20 to 18% moisture content of wheat grains within 3 s is reported by Volchkov et al. [68] (at a non-specified operating temperature). The rate of final drying may, however, remain to be determined by intra-particle diffusion limitations. In later work, Volchkov et al. [69] report values of the heat transfer coefficient for heat transfer between the air and the grain particles. Fig. 26(b) shows measured values as a function of the grain heating time. Model predictions are also shown, where a single particle was considered and a mass-based average grain temperature was used. The latter is strictly only valid for particle Biot numbers below 1. Commercial-scale vortex chamber apparatus for the heating, drying, and cleaning of grain materials were developed, with production rates of 2–30 tons/h [68,69]. For grain drying, the vortex chamber has in certain cases be installed upstream of a shaft dryer used for final drying [69]. Based on a comparison with an existing mining drying apparatus and analyzing the cost reduction by using a 20 tons/h vortex chamber grain heater, 45% increased efficiency and 10% reduced specific expenditures for drying (fuel) are claimed.

An experimental study by Eliaers and De Wilde [31,33] focused on continuous low-temperature drying of pelletized woody biomass. The process intensification was directly evaluated, comparing data from a conventional fluidized bed (FB) dryer and a vortex chamber based high-G fluidized bed dryer (RFB-SG). Details of the experimental set-up are summarized in Table 4. A vortex chamber with λ = 0.107 could be used to dry the ±4 mm diameter wood particles. No separate solids outlet was foreseen and the dried biomass was collected in a specially designed chimney. The wet biomass was fed through a perforation in the end wall opposite the chimney outlet. The specific biomass feed rate, that is, per m^3 drying chamber, versus the mean biomass moisture content at the outlet (chimney), is shown in Fig. 27 and illustrates the factor 7 process intensification that could be achieved by making use of a vortex chamber in a wide biomass outlet moisture

Table 8
Simulation of the simultaneous adsorption of SO_2 and NO_x in a riser and in a vortex chamber. (a) Reactor volume and operating conditions. (b) Process Intensification summary. (From Ref. [6]).

(a)

		GSVR simulation cases			
	Riser	Direct riser comparison	5.38 kg bed no recycle	5.38 kg bed with recycle	Batch operation
Independent basis variables					
Reactor volume (m^3)	24.2	0.023	0.023	0.023	0.023
Total gas feed flow rate (kg/s)	4.84	0.495	0.495	0.495	0.495
Regenerated solids feed rate (kg/s)	1.01	0.103	0.103	0.103	
Recycle ratio (kg_{recyc}/kg_{regen})	3	3		3	
Solids hold-up (kg)	22.0	2.27	5.38	5.38	2.27 or 5.38
Derived quantities					
Gas-to-regenerated solids (kg_{gas}/kg_{regen})	4.8	4.8	4.8	4.8	
Gas-to-total solids fed (kg_{gas}/kg_{solids})	1.2	1.2	4.8	1.2	
Space-time (kg_{solids} s/mol)[a]	68	69	160	160	69 or 160
Weight hourly space velocity (1/h)[b]	2.8	2.8	1.2	1.2	2.8 or 1.2
Solid residence time (s)[c]	22	22	50	50	22 or 50
Solids loading ($kg/m^3_{reactor}$)	0.9	100	230	230	100 or 230
Gas–solid contact time (s)	4.1	~0.005	~0.01	~0.01	~0.005 or 0.01

(b)

		GSVR simulations			
	Riser	Direct riser composition	Delta	5.3 kg bed w/o recycle	Delta
Removal efficiency					
SO_2 (mol/kg_{solids})[d]	0.21	0.21	0.5%	0.23	10%
NO_x (mol/kg_{solids})[d]	0.066	0.073	11%	0.074	12%
SO_2 ($mol/m^3_{reactor}$ s)	0.0086	0.93	~110*x*	1.02	~120*x*
NO_x ($mol/m^3_{reactor}$ s)	0.0027	0.33	~120*x*	0.33	~120*x*
Other parameters					
volume (m^3)	24.2	0.23[e]	~105*x*	0.23[e]	~105*x*
mass transfer coefficient (m/s)	0.06–0.12	1.0–1.1		1.0–1.1	
slip velocity (m/s)	0.2–0.5	6–7		6–7	
bed pressure drop (kPa)	~0.4	~9		~17	

[a] Space–time is defined as the mass of solids in the reactor divided by the inlet molar flow rate of contaminants.
[b] WHSV is defined as the inlet mass flow rate of contaminants divided by the mass of solids in the reactor.
[c] Solids residence time is defined as the solids loading divided by the regenerated solids feed rate.
[d] Defined as the moles adsorbed per second divided by the fresh sorbent feed rate to the reactors.
[e] GSVR volume multiplied by ~10 to achieve the same gas flow rate as the riser.

content range. Only at very low biomass outlet moisture content, intra-particle diffusion limitations become limiting. For the operating conditions studied, the process intensification mainly resulted from an increased particle bed density and improved particle bed uniformity. The coefficients of interfacial mass and heat transfer could only achieve slightly higher values in the vortex chamber than in the conventional fluidized bed because of limitations on the air flow rate (compressor). The contribution of aerodynamic blow off was also found minor. Because a vortex chamber is typically operated at high gas flow rate, the air utilization is to be evaluated. Fig. 28 shows that for a given biomass outlet moisture content, an equal increase of the air humidity can be achieved in the vortex chamber than in the conventional fluidized bed, despite the higher air flow rate. This is explained by the higher biomass feed rate that can be handled by the vortex chamber based dryer, even though its volume is significantly smaller than that of the conventional fluidized bed dryer (see Table 4). Eliaers and De Wilde [31,33] demonstrated the importance of the solids inlet and outlet design and effects on the product quality. Fig. 29 shows an example of the distribution of the biomass moisture content at the outlet and illustrates that part of the biomass fed can bypass the particle bed and be directly entrained into the chimney. Fig. 29 also reveals that the particle bed was not really well-mixed with the applied vortex chamber design and operating conditions, despite the fast particle bed rotation. The axial motion of the biomass from the solids inlet in the end wall opposite the chimney outlet to that chimney outlet cannot be neglected in this case and contributes to an improved product uniformity.

5.2. Low-temperature, wet coating of cohesive particles

Particle coating is used in the feed and food, chemical, pharmaceutical, cosmetic and agricultural industries, for example to protect the core material from contact with ambient air or light, to control the release of an active component, to modify the particle surface properties, or to mask odor or bad taste. Fluidized bed wet spray coating processes are frequently used. The coating material, dissolved or diluted in a solvent, is sprayed on the core material leaving one or multiple coating layers on the particle surface after evaporation of the solvent into the fluidization gas, commonly air [17,61,75]. The use of a fluidized bed ensures efficient mixing and intra- and interfacial contacts. Top, bottom and tangentially sprayed fluidized bed coaters are used. Bottom sprayed so-called Wurster coaters offer an increased coating efficiency by the use of an insert and air distributor. They introduce pronounced particle circulation and improve the contact between droplets and particles.

The above mentioned technologies fluidize the bed against the earth gravitational field and suffer from the limitations already discussed in Section 1. In particular cohesive (Geldart-C type) particles cannot be processed, as a result of dominating Van der

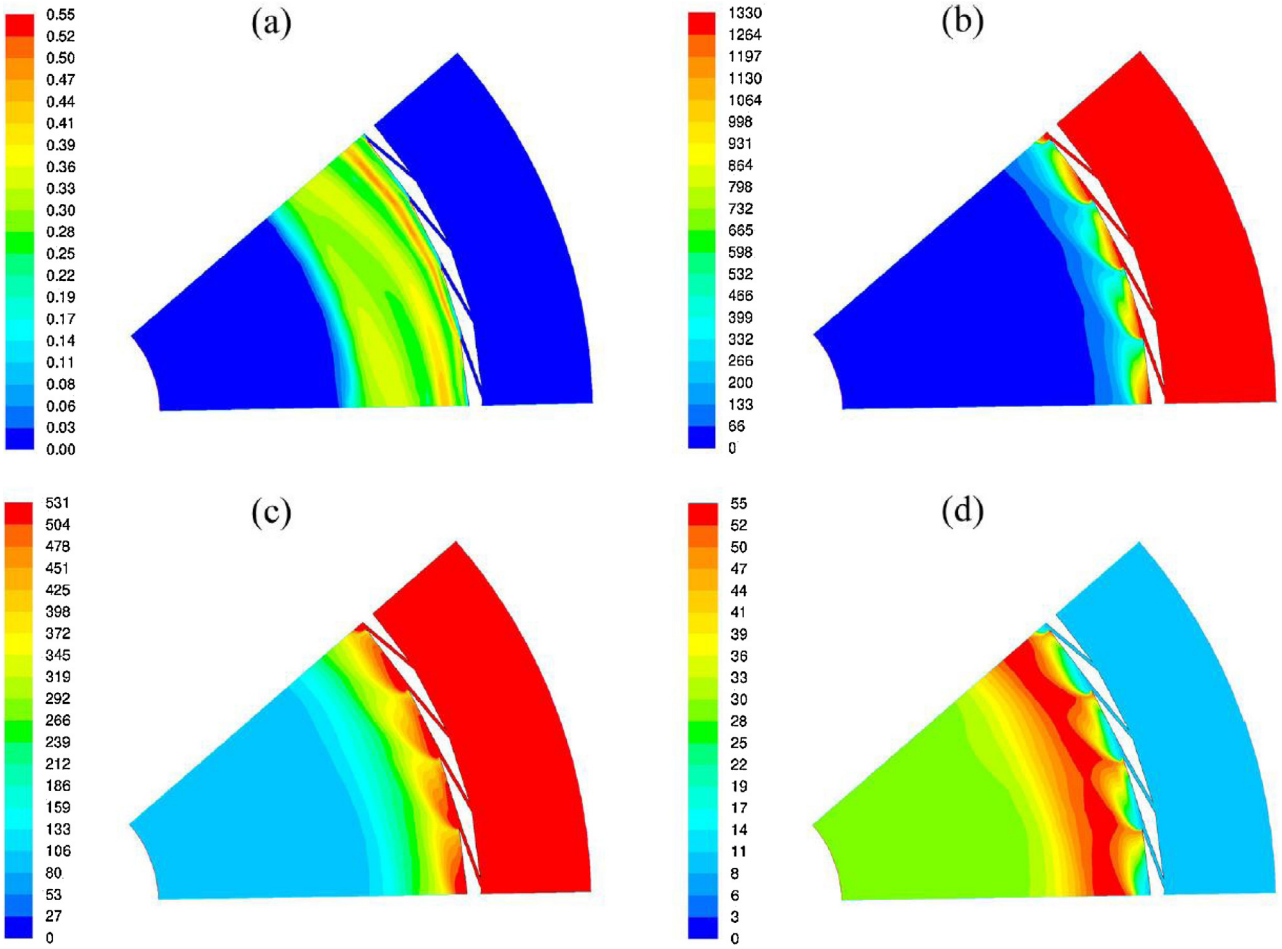

Fig. 32. 2D periodic domain CFD simulations of the simultaneous adsorption of SO_2 and NO_x on a γ-Al_2O_3 sorbent in a vortex chamber type reactor. Snapshot of the (a) solids volume fraction and the (b) SO_2, (c) NO and (d) NO_2 concentrations (ppm-v). Reactor volume and operating conditions: see Table 8(a) – 5.38 kg bed, single-pass case. (From Ref. [6]).

Table 9
Application of high-G gas–solid fluidized beds in vortex chambers and reported process intensification potential.

Application	Reference technology	Process intensification effect(s)	Process intensification mechanisms	Type of study & references
Biomass drying	Conventional fluidized bed	-Reduced residence time (batch) -Reduced chamber volume (continuous) -About one order of magnitude PI -Independent control of the gas & solids residence time-Geldart A,B,C and D-type particles -Multi-zone operation facilitated	-Increased bed density -Improved bed uniformity -Increased gas–solid slip velocities => Intensified interfacial mass, heat & momentum transfer	Experimental, pilot & commercial scale: -[43,44] -[68,69] -[28] -[11–13,15] -[33] -[30]
Fluid catalytic cracking of gas oil SO_2 NO_x adsorption process Biomass pyrolysis & gasification	Circulating fluidized bed riser	-Reduced chamber volume -One to two orders of magnitude PI -Independent control of gas and solids residence time -Extremely short gas–solid contact time possible -Multi-zone operation facilitated	-As above Patents for all three applications: -[11–13,15] -[14]	Numerical: -[62,65] Numerical: -[6] Numerical: -[59] -[5] Commercialized: -Synvalor BV, The Netherlands
Particle coating	Spouted bed wurster coater	-Reduced coating time -Also applied to Geldart C-type particles -Fluidization maintained at high liquid droplet concentration -Agglomeration controlled by means of the gas flow rate	As above & -Increased gas–liquid slip velocities -High particle bed rotation speed & intensified particle bed mixing -Flexibility in the gas flow rate	Experimental, pilot scale: -[11–13,15] -[32,34]

Waals forces. Also, pronounced agglomeration or granulation can be observed when relatively large droplets are introduced, that is, compared to the particles that are coated [17,8]. To reduce the importance of the Van der Waals forces, modification of the particle surface properties, e.g., by dry-coating with nano-particles [8], or fluidization in a high-G field can be considered. The latter allows intensifying interfacial momentum transfer, besides interfacial mass and heat transfer. The use of a rotating chamber was studied by Watano et al. [72,73].

Eliaers and De Wilde [32] and Eliaers et al. [34] demonstrated the low-temperature wet coating of cohesive particles in a vortex chamber equipped with a centrally positioned single-fluid pressure spray nozzle directed towards the bed. Semi-continuous experiments were carried out. Continuous feeding of (uncoated) particles was required to compensate losses via the chimney. At time t_0, coating was started. After a given coating time, both the liquid and solids feeding were stopped after which the coated particles were recuperated from the vortex chamber. SEM imaging, laser diffraction based particle size distribution measurements and an active component release test were used to analyze agglomeration and the particle coating quality. No coated particles were lost via the chimney.

To be able to fluidize the cohesive particles, a vortex chamber with 72 gas inlet slots, 0.2 mm wide each had to be used. The diameter of the vortex chamber was 0.24 m, so that $\lambda = 0.019$. Details of the operating conditions are given in Table 5. The experiments also revealed that the presence of a dispersed liquid phase in too high concentrations can be detrimental for the bed stability and can lead to defluidization and slugging. Within a sufficiently wide liquid feed rate range and coating time range, a stable, dense and relatively uniform rotating fluidized bed could, however, be maintained.

The experiments showed that agglomeration can be controlled by means of the gas flow rate (Fig. 30), taking advantage of the flexibility with respect to the latter of rotating fluidized beds in vortex chambers (see Section 3.3). High gas–solid slip velocities and high shear in the rotating particle bed can as such be generated to reduce agglomeration. Increasing the liquid solution injection pressure results in an increased liquid feeding rate, but smaller droplets. Eliaers et al. [34] observed that the latter prevents uncoated particles to be entrained by the gas into the chimney, significantly increasing the overall coating efficiency while hardly affecting agglomeration. The analysis of the quality of less and more agglomerated coated particles is summarized in Table 6. For

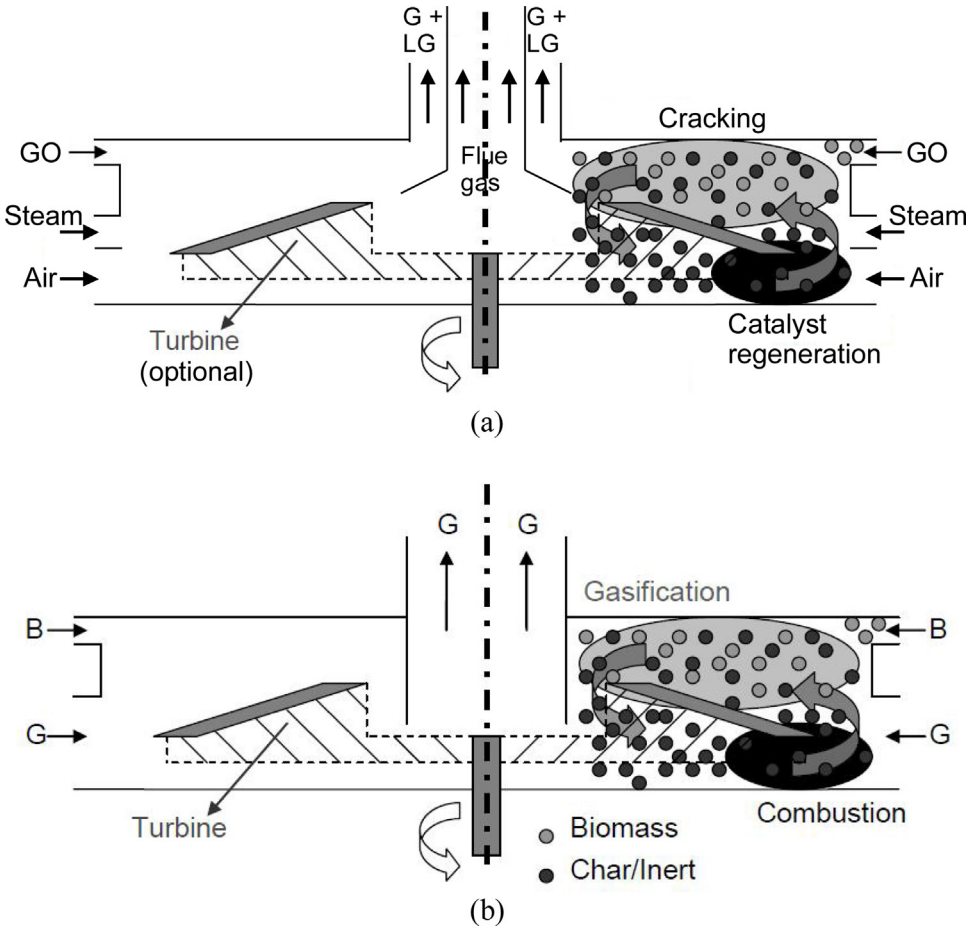

Fig. 33. Illustration of axial multi-zone operation in a vortex chamber and the generation of a circulating rotating fluidized bed (CRFB) (left part of the reactors presented without particles). (a) Example of fluid catalytic cracking of gas oil with integrated cracking and catalyst regeneration zones, separated by steam injection. Cracking products and flue gas evacuated separately by means of a dual-chimney. (b) Example of low-temperature pyrolysis and gasification of biomass. Two different reaction zones are introduced: a char combustion zone and an anaerobic biomass pyrolysis zone. Char (and eventually inert sand) is circulating longitudinally between the two reaction zones. A double chimney design is also possible. (From Ref. [59]).

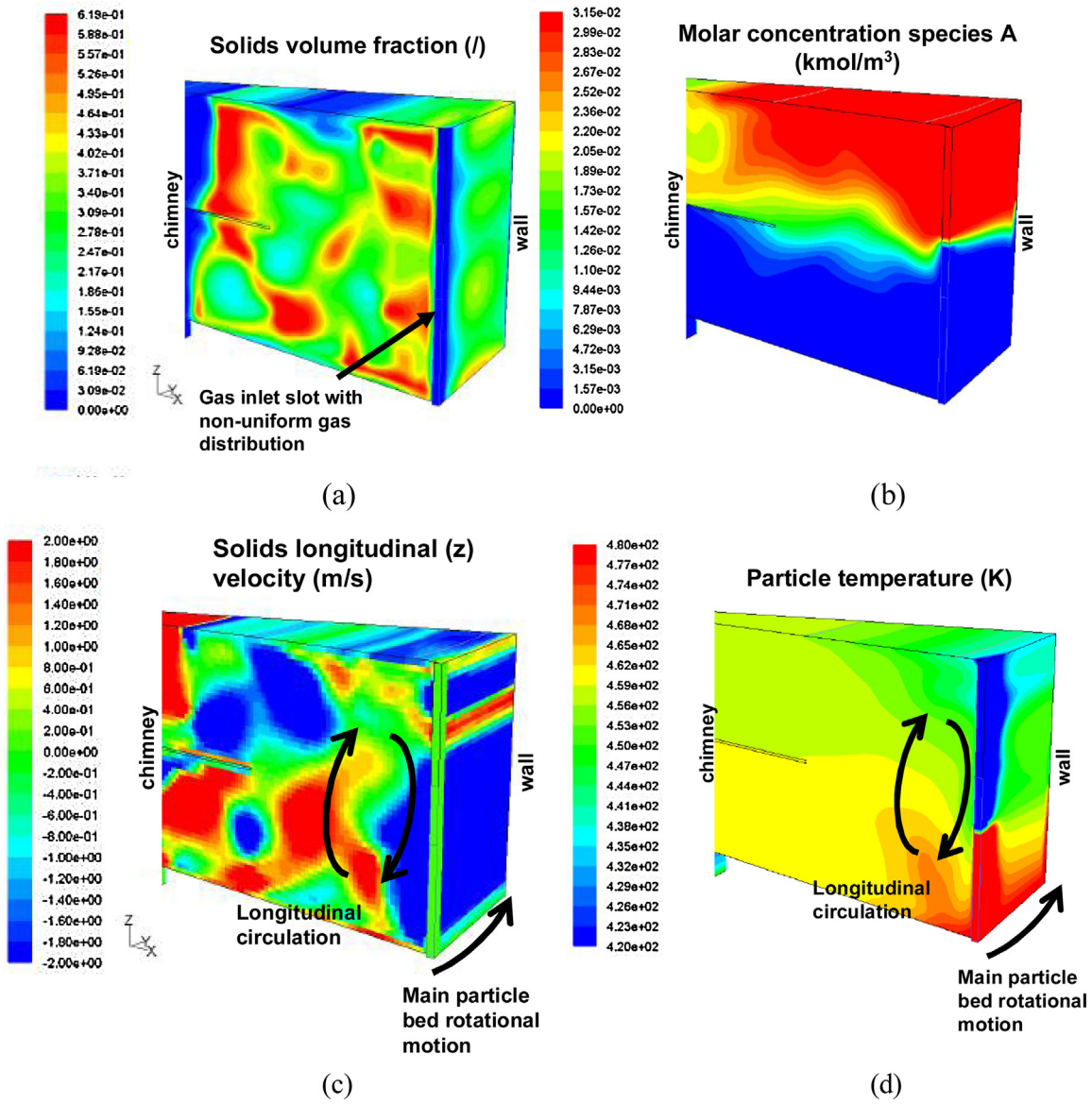

Fig. 34. 3D periodic domain CFD simulations of a circulating rotating fluidized bed (CRFB), illustrating the axial–radial circulation of solids, the particle bed temperature uniformity and the separation of the gases injected in different zones of the vortex chamber. Profiles of the (a) solids volume fraction, (b) gas composition, (c) axial solids velocity, and (d) particle bed temperature. Vortex chamber with $D = 240$ mm and $L = 50$ mm. Cold gas A injected at 300 K via the top section of the gas inlet slot, hot gas B injected at 950 K via the bottom section of the gas inlet slot. (Adapted from Ref. [59]).

both, a good quality coating could be fast and relatively efficiently produced in the small-volume vortex chamber type particle coater.

5.3. Fluid catalytic cracking (FCC)

Fluidized beds offer excellent heat transfer properties and the possibility of circulating the particles, allowing for example continuous regeneration of a fast deactivating catalyst. The main application is fluid catalytic cracking (FCC) of (vacuum) gas oils, developed in the early forties. Other fluidized bed processes for carrying out heterogeneous catalytic and non-catalytic reactions have been commercialized since. As explained in Section 1, conventional fluidized beds suffer from limitations with respect to the range of operating conditions and the dimensions due to the role of earth gravity in their operation. FCC is carried out in a fluidized bed or, in modern units, in a riser within a circulating fluidized bed (CFB) system [38]. At the top of the riser, gas and solids are efficiently separated by means of a battery of cyclones. The particles return downward via standpipes, a stripper and a regenerator. The downward motion in the standpipes is driven by the hydrostatic pressure and requires a sufficient standpipe height. The riser should be sufficiently tall to accommodate the cyclones, the standpipes and the regenerator system. The catalyst that can be used, i.e., its activity, and to a certain extent the operating temperature are determined by the riser height. Overcracking should be avoided. Furthermore, riser reactors are dilute, with of the order of 2–5 vol% particles, and the gas–solid slip velocity is limited by the terminal velocity of the particles in the earth gravitational field.

The use of a vortex chamber to generate a rotating fluidized bed in a static geometry (RFB-SG) allows overcoming the limitations of conventional fluidized beds. Because the particle bed in RFB-SGs is relatively thin – of the order of centimeters – and the gas velocities are high, the gas phase residence time in the particle bed is much smaller than in a conventional fluidized bed or in a riser. To compensate for this and allow a

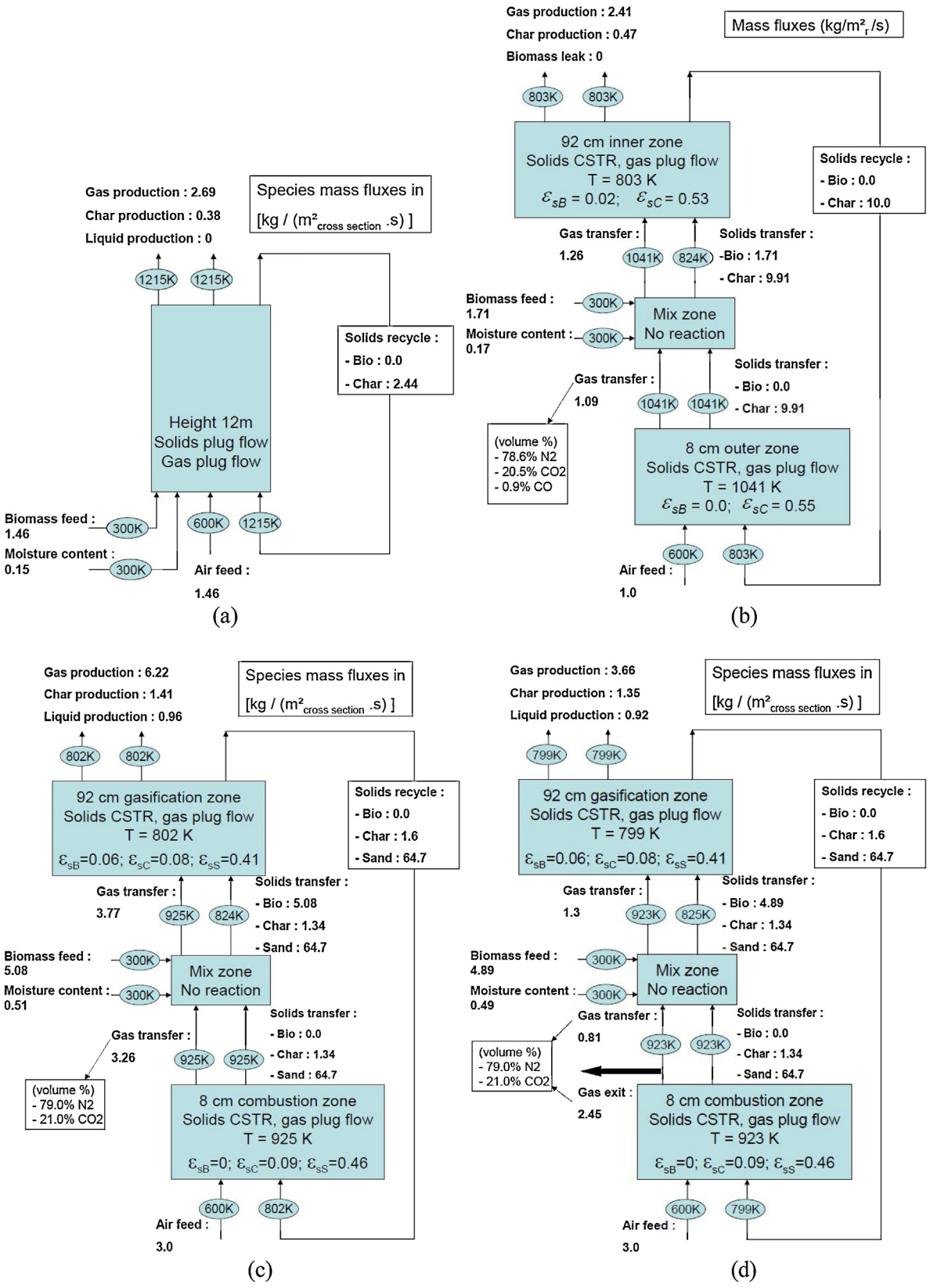

Fig. 35. 1D simulation of low-temperature pyrolysis and gasification of biomass in a (a) circulating fluidized bed (CFB) riser; (b–d) circulating rotating fluidized bed (CRFB – see Figs. 33(b) and 34) operating at a temperature below the ash melting temperature. (a and b) Char recycle only; (c and d) char and inert sand recycle. (a–c) Single gas outlet/chimney; (d) dual-chimney design for a separate evacuation of the production and flue gases. Operating conditions given in the figures. (From Ref. [59]).

sufficiently high conversion, RFB-SGs offer a higher particle bed density, improved particle bed uniformity and intensified interfacial mass and heat transfer. Trujillo and De Wilde [62,65] calculated by means of detailed CFD simulations, including the 10-lump kinetic model of Jacob et al. [42], the conversion and process intensification that could be achieved when catalytically cracking gas oil in a RFB-SG. The objective of the study was to demonstrate that sufficiently high conversions can be achieved in a very short gas–solid contact time and a non-optimized vortex chamber design was used. In order to ensure the generation of a sufficiently dense bed of the Geldart A-type catalyst powder, the vortex chamber was designed with a λ of 0.01. Fig. 31 shows that for the typical commercial operating conditions and the vortex chamber design summarized in Table 7, sufficiently high conversions can be achieved. A comparison with a riser type reactor is also shown in Fig. 31, confirming the about one order of magnitude process intensification resulting from the use of a RFB-SG. A process intensification (PI) factor was defined based on the bed height and corresponding reactor volume required to achieve a given gas oil conversion for the given flow rate, and this, based on the calculated solids volume fraction and species concentration profiles:

$$\mathrm{PI}(\chi_{GO}) = \frac{X_G^{RFB}(\chi_{GO})}{X_G^{riser}(\chi_{GO})} \quad \text{where :} \quad X_G(\chi_{GO}) = w_G(\chi_{GO}) \times \frac{m^{GO}}{V(\chi_{GO})}$$

and $w_G(\chi_{GO})$ is the gasoline mass fraction produced for given gas oil feed rate, m_{GO}, and gas oil conversion, χ_{GO}. $V(\chi_{GO})$ is the particle bed volume required to achieve this gas oil conversion at the given gas oil feed rate. Fig. 31(b) shows the PI factor as a function of the gas oil conversion. The achieved process intensification is explained by a combination of increased bed density, improved particle bed uniformity and intensified interfacial mass and heat transfer. Typical profiles of the solids volume fraction in the RFB-SG and riser reactors simulated are shown in Fig. 31(c). The jump in the PI factor is explained by the two-peak solids volume fraction

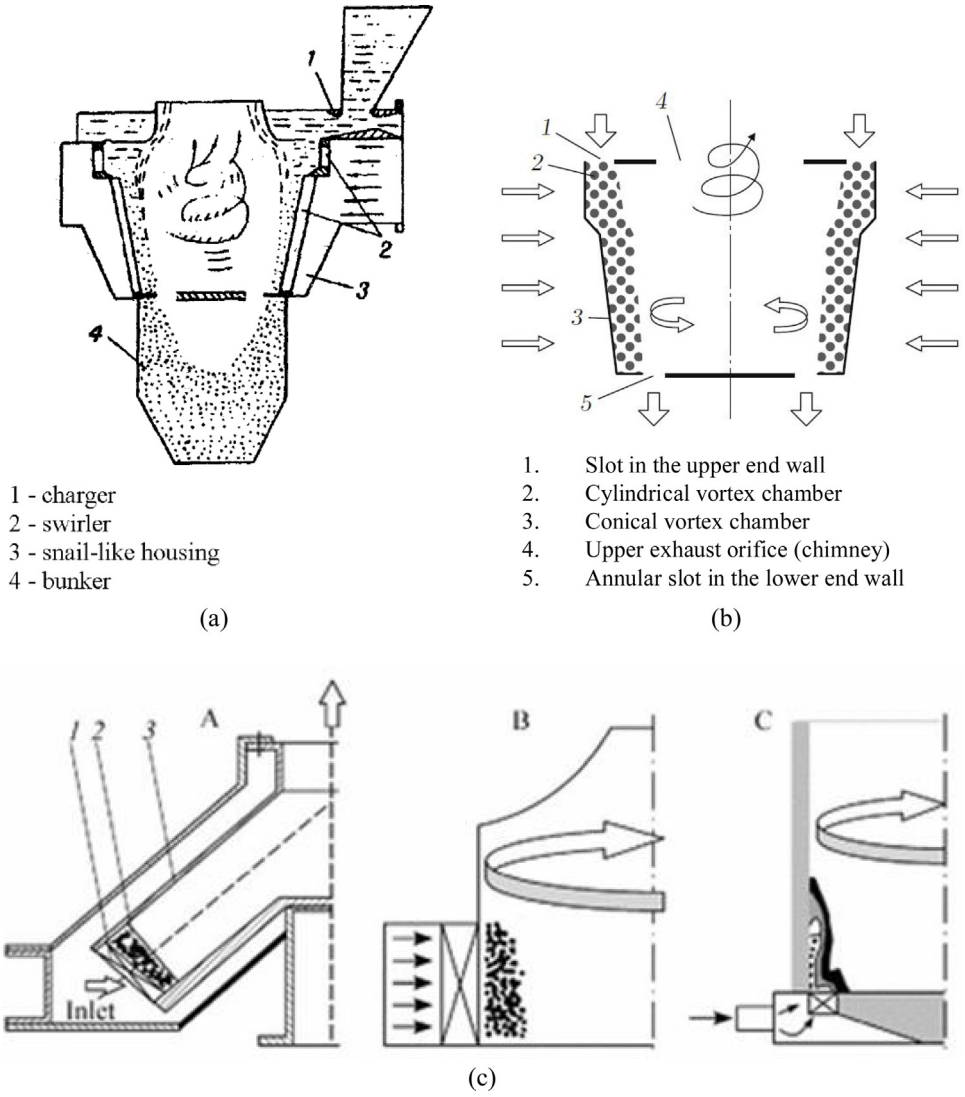

Fig. 36. (a and b): Hybrid design with cylindrical and conical vortex chambers used for grain drying. (a) From [69]; (b) adapted from Ref. [28]. (c) Different designs considered for the combustion of an air–fuel (propane–butane) mixture. Left: conical chamber; middle: cylindrical chamber; right: lateral slot swirler (Torbed). (1) Slot swirler; (2) particle bed; (3) chamber shell. (From Ref. [71]).

profile. Note that higher conversions could be achieved in the RFB-SG by optimizing its design.

Additional process intensification can be realized by the use of a more active catalyst and/or operation at higher cracking temperatures – both also made possible by the short gas phase residence time and the very efficient particle bed mixing and resulting particle bed temperature uniformity in a RFB-SG [62]. In later work, different vortex chamber designs were evaluated, as discussed earlier (see Fig. 20) [64,65].

5.4. SO_2 NO_x adsorption process (SNAP)

Ashcraft et al. [6] considered the use of a vortex chamber type reactor for the simultaneous removal of SO_2 and NO_x by adsorption on a γ-Al_2O_3 sorbent (SO_2 NO_x adsorption process – SNAP), conventionally carried out in a circulating fluidized bed riser. To calculate the reactor performance, two- and three-dimensional periodic domain CFD simulations were carried out including the detailed kinetic model of De Wilde et al. [18] and accounting for interfacial mass transfer limitations. The process intensification was evaluated by comparison with the commercial scale riser simulations of Das et al. [10]. The vortex chamber studied had a diameter of 0.54 m, a chimney diameter of 0.15 m and a length of 0.1 m. Flue gas at 0.6 m^3/s was introduced through 36 slots, 2 mm wide each, so that $\lambda = 0.042$. The gas fed contained 1330 ppm SO_2, 531 ppm NO, 10 ppm NO_2, 20,000 ppm O_2 and N_2. Isothermal operation at 414 K was imposed. Two sorbent particle diameters were used, 70 and 200 μm, but only minor differences in the behavior are reported. Different cases were simulated, including batch-wise and continuous operation for the sorbent. In the latter case, fresh sorbent ($\rho_s = 1550\ kg_{sorbent}/m^3_{sorbent}$, site density = $0.928\ mol_{site}/kg_{sorbent}$) was fed at 0.103 kg/s to operate at equal gas-to-fresh sorbent feed ratio as in the riser simulations by Das et al. [10], i.e., 4.8 $kg_{gas}/kg_{sorbent}$. Partial recycle of the sorbent was also considered with a recycle ratio of 3:1 as in Das et al. [10]. When using a riser reactor, such partial sorbent recycle is necessary to use the sorbent optimally. With a vortex chamber, the solids residence time can be controlled independently of the gas flow rate and sorbent recycle can eventually be eliminated. For the same reason, Ashcraft et al. [6] could, at equal solids feeding rate, consider two possible solids loadings in the vortex chamber, 2.27 kg, giving an equal solids loading-to-gas flow rate ratio as in the riser simulations of Das et al. [10], and 5.38 kg, resulting in a more realistic bed height. Table 8(a) summarizes the reactor volume and operating conditions for the riser and vortex chamber SNAP simulations. The different scale of the riser and vortex chamber units should be noted. The simulated vortex chamber was designed for a flue gas flow rate about 10 times smaller than that of the simulated riser. The vortex chamber volume was, however, about 1000 times smaller.

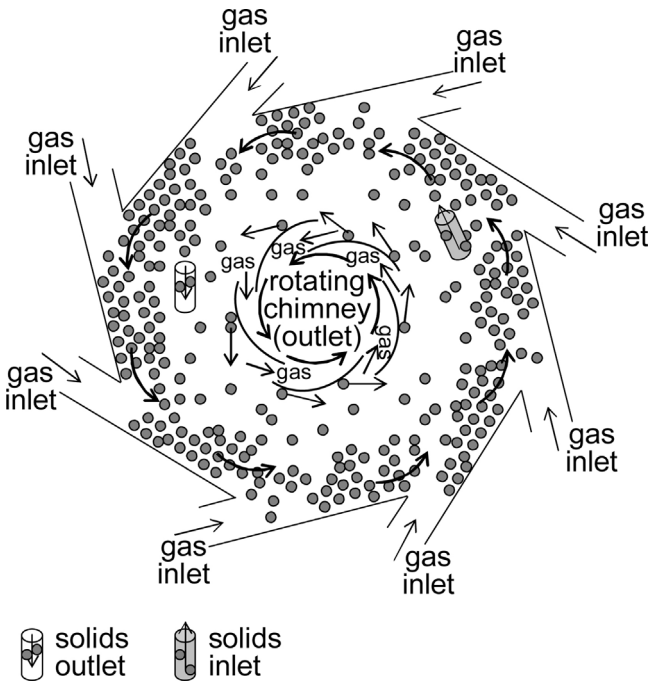

Fig. 37. Integration of a rotating chimney in a vortex chamber. (From Ref. [23]).

With a 2.27 kg solids loading in the vortex chamber, the removal efficiencies for SO_2, NO and NO_x are, respectively, 91%, 84% and 79%. For SO_2, this is comparable to the removal efficiency achieved in a riser reactor. For NO and NO_x the removal efficiency is significantly better (76%, respectively, 71% are reported by Das et al. [10]. Operation at higher solids loading, i.e., 5.38 $kg_{sorbent}$, allows further increasing the SO_2, NO and NO_x removal efficiencies to respectively 99.7%, 85% and 80%. Typical profiles of the solids volume fraction and the SO_2, NO and NO_2 concentrations are shown in Fig. 32. The simulations of Ashcraft et al. [6] confirm that, thanks to a high bed density and improved bed uniformity, sufficiently high conversions can be achieved in the relatively thin rotating fluidized bed, despite the high gas velocities and related short gas-solid contact time. The simulations also reveal that, in the range of operating conditions studied, the solids residence time can be easily optimized, so that solids recycle hardly affects the vortex chamber reactor performance.

The process intensification that can be achieved by using a vortex chamber reactor instead of a riser is summarized in Table 8(b). It was assumed that, without affecting the performance, the vortex chamber reactor could be scaled up by a factor 10, so that an equal gas flow rate as in the riser simulations of Das et al. [10] can be treated. Table 8(b) shows that 2 orders of magnitude process intensification can be achieved, mostly as a result of the increased bed density. Much higher gas–solid slip velocities than in the riser allow intensifying interfacial mass transfer by easily one order of magnitude, but the latter is not really rate determining in the SNAP case. High-G operation comes at the cost of a somewhat increased pressure drop over the particle bed, about a factor 20 at equal solids loading-to-gas flow rate ratio.

An overview of the different case studies discussed in this section is given in Table 9. It is clear that within a wide variety of applications, the use of a high-G fluidized bed in a vortex chamber offers a significant process intensification potential. This not only allows significantly reducing the chamber or reactor size, with the resulting positive effects on cost and safety, but also to carry out processes that are difficult or impossible to carry out when fluidizing against earth gravity. The independent control of the gas and solids residence time is an additional advantage when comparing to a circulating fluidized bed riser. The intensification of interfacial mass, heat and momentum transfer is at the origin of the process intensification. The latter allows dense beds at high gas–solid slip velocities and the fluidization and processing of cohesive particles. It also leads to an improved bed uniformity. Finally, it should be stressed that in order to take fully advantage of the process intensification potential of a vortex chamber fluidized bed reactor, the use of a more active catalyst or operation at higher temperatures should be considered.

6. Multi-zone operation, extensions of the concept and combination with a rotating chimney or spinning disc

Multi-zone operation can be easily realized in vortex chambers, either in the tangential (Fig. 5) or axial (Fig. 33) direction. Gases

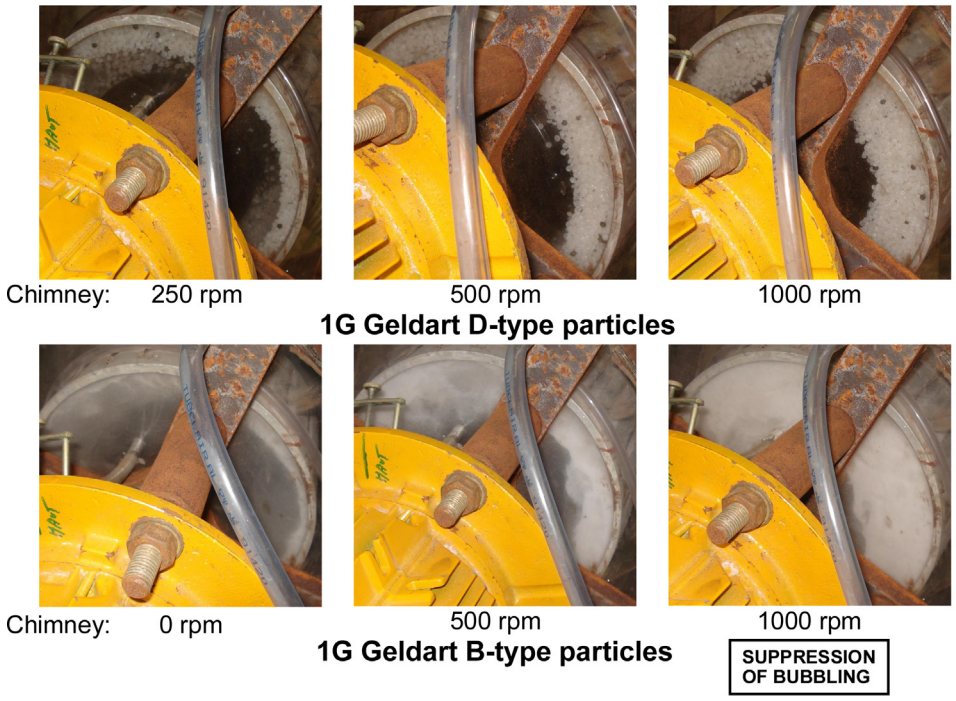

Fig. 38. Vortex chamber with integrated rotating chimney. (a) Influence of the chimney rotation speed on the solids loading and particle bed density and uniformity in a RFB-SG operated at given gas and solids feeding rates and feeding 2–5 mm polymer pellets (top) and 300 μm salt particles (bottom). Suppression of bubbling at high solids loadings of 300 μm salt due to compression of the particle bed by the rotating chimney. (b) Pressure drop over the particle bed as a function of the solids loading when fluidizing 300 μm salt particles with a chimney rotating at 1000 rpm, again illustrating compression of the particle bed at high solids loadings. Vortex chamber design: see Fig. 3. (From Ref. [24]).

that differ in composition and/or temperature can as such be injected via the different gas inlet slots or different parts of the gas inlet slots, allowing integration of different reaction zones into the vortex chamber. The injection of a very hot gas in part of the vortex chamber allows, for example, the supply of sufficient heat to the particle bed while limiting the time of high-temperature exposure. As shown by CFD simulations and experimental measurements, gradients in the particle bed temperature remain remarkably small by efficient mixing, even with extreme differences in the gas feed temperatures in different zones of the vortex chamber (Fig. 34) [59]. Particle coating with an axially non-uniform heat supply was experimentally studied by Eliaers and De Wilde [32].

As an extension of the rotating fluidized bed in a static geometry (RFB-SG), the concept of a circulating rotating fluidized bed (CRFB) was developed. On the top of the particle bed rotational motion, an axial-radial circulation is introduced in the particle bed. Such a circulation occurs naturally in RFB-SGs as a result of the axial gradients in the particle bed rotation velocity in the vicinity of the end walls [32], but can be intensified by an axially non-uniform gas distribution or a rotating chimney, discussed later. Application of the CRFB concept to fluid catalytic cracking and to the low-temperature pyrolysis and gasification of biomass are schematically illustrated in Fig. 33. Three-dimensional periodic domain CFD simulations by Staudt et al. [59] demonstrated the effect of an axially non-uniform gas distribution, both in composition and temperature (gas A fed at 300 K, gas B at 950 K). Interestingly, the significant axial motion/circulation introduced in the particle bed results in minimal axial mixing in the gas phase. Fig. 34 shows the resulting quite uniform particle bed temperature, despite the 650° temperature difference of the different gases injected. Sufficient heat could, however, be supplied to the bed. The minimal axial mixing of gases A and B is explained by the high radial gas velocity and allows separate evacuation via two chimneys (eventually also of gases produced in the different axial zones). The chimneys can be connected to the opposite end walls or integrated in one of the end walls (Fig. 33). Fig. 34 illustrates the separate evacuation of gases A and B.

The potential of using a RFB-SG or CRFB for carrying out the low-temperature pyrolysis and gasification of biomass was also numerically evaluated by Staudt et al. [59]. A CRFB is particularly suited for axial multi-zone operation and allows integrating a biomass pyrolysis zone and a char combustion zone, as shown in Fig. 33(b). By the axial–radial circulation introduced in the particle bed, the solids (char eventually mixed with a high heat capacity inert solid, typically sand) move in a closed loop between both reaction zones. The char recycle rate can, hence, be very high. The heat required for the biomass pyrolysis can as such be supplied by the combustion of the char. To prevent air burning the gas produced by the biomass primary pyrolysis, the fresh air is fed in the char combustion zone. The biomass is injected in between the two reaction zones such that it circulates to the biomass pyrolysis zone first. The temperature difference between the two reaction zones remains small, due to the solids circulation and efficient particle bed mixing. This opens perspectives for carrying out the biomass pyrolysis at higher temperatures, while not exceeding the ash melting temperature (≈900–1100 K) in the char combustion zone.

Staudt et al. [59] simulated the reference circulating fluidized bed (CFB) riser reactor using a 1D plug flow model with slip between the phases. For the RFB-SG and CRFB type reactors, the particle bed was assumed to behave like a completely stirred reactor (CSTR), respectively, a combination of CSTRs, and the gas flow motion to be close to plug flow, in accordance with experimental and CFD observations – see Section 3.6 and Figs. 5 and 9. The effects of the reactions on the hydrodynamics were neglected. A lumped reaction scheme was adopted to describe the pyrolysis and gasification of woody biomass. Particles with an equivalent diameter of 650 μm were considered, small enough to neglect intra-particle diffusion limitations. Interfacial mass and heat transfer limitations were accounted for, as well as a certain feed biomass moisture content. Operation at atmospheric pressure was studied. The CFB riser was 12 m tall, whereas the 'total' bed height in the CRFB was 1 m of which 0.92 m biomass pyrolysis zone. The process intensification can be evaluated from the amount of biomass that can be converted per m^3 reactor and per s, the so-called specific biomass conversion rate. The latter follows from the species mass fluxes (in kg/(m^2 cross section/s)) and the bed height. Fig. 35 shows simulation results for the reference CFB riser and for CRFBs, assuming different operating conditions given in the figure. In the CRFB simulations, the temperature at which the biomass pyrolysis takes place was always limited to 800 K to avoid ash melting in the char combustion zone. If no sand is circulated in the reactor, the specific biomass conversion rate was found to be easily one order of magnitude higher in a CRFB than in the CFB riser. About two orders of magnitude process intensification can be achieved by using a RFB-SG (not shown, see original paper), but in a CRFB the liquids production can be optimized and the char production reduced. The LHV of the produced dry gas (including liquids) was found comparable. Staudt et al. [59] further showed that the circulation of a sand–char mixture allows further increasing the specific biomass inlet flux and specific biomass conversion rate (Fig. 35(c and d)). The product distribution and the LHV of the produced dry gas are hardly affected. In a CRFB, an almost doubling of the LHV of the produced dry gas can be realized by separately evacuating the flue gas (Fig. 35(d)), using a separate gas outlet for the biomass pyrolysis and the char combustion zone, respectively. The significant process intensification that can be achieved is explained by a combination of an increased bed density and increased gas–solid slip velocities resulting in intensified interfacial mass and heat transfer. In later work, Ashcraft et al. [5] modeled the fast pyrolysis of biomass in a rotating fluidized bed in a static geometry. The stratification of the solid phases was shown to allow retaining the sand and unreacted biomass in the vortex chamber. The degree of char formation was found comparable to that in a conventional fluidized bed, but more tar and less pyrolysis gas is produced, confirming the findings of Staudt et al. [59].

Vortex chambers can be cylindrical, conical or hybrid. A grain dryer with a hybrid design is shown in Fig. 36(a and b) [69,28]. Multi-zone operation is possible and the gas composition and flow rate to the different chambers of the grain dryer can be independently controlled. Different types of chambers, including conical, cylindrical and Torbed type have been recently studied with both inert air supply and air-fuel (propane–butane) supply and combustion [70,71]. Schematic representations of such designs are shown in Fig. 36(c). The combination of tangential and axial air injection using a vortex chamber with a perforated end plate was recently studied by Pitsukha et al. [49]. The vortex chamber was operated vertically and under the operating conditions studied the effect of gravity was dominant, so that a high-G cylindrically shaped rotating fluidized bed was not formed. The data in the absence of particles show that the suction normally observed in the radial center of the vortex chamber can be reduced or eliminated by some secondary air injection through the end plate.

A rotating chimney can eventually be integrated in a vortex chamber [46,14], as schematically shown in Fig. 37. The chimney rotates in the same sense as the rotating particle bed, but typically at higher rotation speeds, locally increasing the centrifugal force. For given operating conditions, this allows significantly reducing the rate of solids losses via the chimney. As such, a rotating chimney can be used to control the particle residence time, if necessary. De Wilde and de Broqueville [23,24] experimentally studied the influence of a rotating chimney on the behavior of a rotating fluidized bed in a static geometry, using different types of particles. The rotating chimney in particular allowed suppressing bubbling (Fig. 38(a)). It acts like a compressor on the particle bed at high solids loadings (Fig. 38(b)) and allows widening the range of operating conditions in which a stable, dense and uniform rotating fluidized bed can be obtained. In case of a CRFB, the rotating chimney can be used to control or intensify the axial-radial circulation of the solids. Eliaers and De Wilde [32]

studied the integration of a spinning disc in the vortex chamber for the coating of cohesive particles.

7. Summary and outlook

In vortex chambers, the process gas is injected via multiple slots in the outer cylindrical wall and evacuated via a centrally positioned chimney. This allows the generation of a rotating fluidized bed in a static geometry (RFB-SG). This review deals with the hydrodynamic characteristics, design aspects and applications of gas-solid fluidized beds in vortex chambers.

The cylindrical shape and high-G operation allow the generation of thin particle beds and high specific gas flow rates, resulting in extremely short gas phase residence times in the particle bed. High-G operation also allows maintaining a dense and more uniform particle bed at high gas–solid slip velocities, intensifying interfacial transfer of mass, heat and momentum. The latter improves the fluidization behavior of cohesive particles and in the presence of a dispersed liquid phase. The flexibility with respect to the gas flow rate is remarkable and explained by its similar effect on the centrifugal force and the counter-acting radial gas–solid drag force. A sufficiently high solids loading is required to obtain a stable, dense and uniform rotating particle bed. At too low solids loadings, channeling and slugging occur. The tangential fluidization ensures efficient mixing in the particle bed. The bed can, but does not have to be radially fluidized. Mixing of gases injected via different gas inlet slots or via different parts of the gas inlet slots within the vortex chamber can be kept minimal, facilitating multi-zone operation.

A careful vortex chamber design is required, in particular when fluidizing fine or light particles. The reported guidelines for dimensioning a vortex chamber should be used with caution. Computational fluid dynamics simulations are required for an accurate design and in particular for calculating the particle bed rotation speed resulting from the gas injection. With respect to the latter, the gas inlet and outlet (chimney) design are shown to be critical. Increasing the gas injection velocity for a given gas flow rate, by reducing the number of slots or their size, allows increasing the ratio of the centrifugal force and the radial gas–solid drag force, improving the bed stability and uniformity, increasing the bed density and reducing the solids losses via the chimney. To ensure maximum tangential momentum transfer between the gas injected and the solids, the gas inlet slot size should, however, always exceed the particle size. A minimum number of slots is also required to ensure a uniform gas distribution in the chamber. Extremely small gas inlet slots are, however, required to fluidize light particles. The chimney design is equally important. A small-diameter chimney allows taking advantage of the Coriolis effect to return radially entrained particles back to the particle bed before being lost into the chimney. The formation of a free vortex type flow pattern in the particle bed freeboard region intensifies this effect. Both a reduction of the gas inlet and outlet surface area to improve operation with light particles comes at the cost of an increased pressure drop over the vortex chamber. The solids can be fed via the end walls, via some of the gas inlet slots or via separate slots. Normally, the tangential momentum supplied through the solids feeding should be negligible. The solids feeding can have an important influence on the particle bed stability and uniformity. Furthermore, direct entrainment of the solids into the chimney, bypassing the particle bed, is to be avoided. When continuously feeding solids, they can be removed together with the gas via the chimney for downstream separation or via separate solids outlets, taking advantage of the gas-solids separation inside the vortex chamber. The latter allows a separate control of the gas and solids residence times in the vortex chamber and was shown to improve the particle bed stability, rotation speed and density by reducing the solids concentration in the particle bed freeboard region, allowing the generation of a free vortex type flow pattern in this region. Solids losses via the chimney can, however, not always be eliminated.

The use of vortex chambers for drying granular materials was experimentally and numerically studied by different groups. Process intensification is achieved due to a combination of increased particle bed density, improved particle bed uniformity and increased gas–solid slip velocities resulting in more efficient interfacial mass and heat transfer. The latter is contributing to a less extent towards final drying of the particles when intra-particle diffusion limitations are encountered. More recently, the coating of light (cohesive) particles was experimentally demonstrated. Within a sufficiently wide liquid concentration range, a stable and relatively dense and uniform rotating fluidized bed could be maintained and high-quality coatings could be produced. Agglomeration could be controlled by means of the gas flow rate, taking advantage of the flexibility with respect to the latter. A careful liquid droplet spray design allows significantly reducing the loss of uncoated particles into the chimney and increasing the overall coating efficiency. The extremely short contact time between the process gas and the particle bed opens perspectives for carrying out certain heterogeneous catalytic reactions. The potential process intensification was numerically demonstrated and can be boosted by the use of a more active catalyst or operation at higher temperature. This is possible by the remarkable particle bed temperature uniformity resulting from the pronounced particle bed mixing.

Finally, the vortex chamber concept can be extended in different ways. Cylindrical, conical and hybrid systems have been developed. Tangential and axial multi-zone operation is possible and an axial-radial circulation of particles can be superimposed on the main particle bed rotational motion and controlled by means of a non-uniform distribution of the process gas. A rotating chimney or spinning disc can also be integrated into the vortex chamber to increase the operating flexibility.

References

[1] K. Agrawal, P. Loezos, M. Syamlal, S. Sundaresan, The role of meso-scale structures in rapid gas–solid flows, J. Fluid Mech. 445 (2001) 151–185.

[2] A. Ahmadzadeh, H. Arastoopour, F. Teymoour, Rotating fluidized bed an efficient polymerization reactor, AIChE Annual Meeting, Cincinnati, OH, USA, 2005.

[3] L.A. Anderson, S. Hasinger, B.N. Turman, Two Component Vortex Flow Studies, with Implications for the Colloid Core Nuclear Rocket Concept, A.I.A.A Paper, 71 (637) (1971).

[4] L.A. Anderson, S.H. Hasinger, B.N. Turman, Two-component vortex flow studies of the colloid core nuclear rocket, J. Spacecr. Rockets 9 (5) (1972) 311–317.

[5] R.W. Ashcraft, G.J. Heynderickx, G.B. Marin, Modeling fast biomass pyrolysis in a gas–solid vortex reactor, Chem. Eng. J. 207 (208) (2012) 195–208.

[6] R.W. Ashcraft, J. Kovacevic, G.J. Heynderickx, G.B. Marin, Assessment of a gas–solid vortex reactor for SO_2/NO_x adsorption from flue gas, Ind. Eng. Chem. Res. 52 (2013) 861–875.

[7] Y.-M. Chen, Fundamentals of a centrifugal fluidized bed, AIChE J. 33 (1987) 722–728.

[8] Y. Chen, J. Yang, A. Mujumdar, R.N. Dave, Fluidized bed film coating of cohesive Geldart group C powders, Powder Technol. 189 (2009) 466–480.

[9] R. Chevray, Y.N.I. Chan, F.B. Hill, Dynamics of bubbles and entrained particles in the rotating fluidized bed, AIChE J. 26 (1980) 390–398.

[10] A.K. Das, J. De Wilde, G.J. Heynderickx, G.B. Marin, CFD simulation of dilute phase gas–solid riser reactors: part II – simultaneous adsorption of SO_2–NO_x from flue gases, Chem. Eng. Sci. 59 (2004) 187–200.

[11] A. de Broqueville, Catalytic polymerization process in a vertical rotating fluidized bed. Belgian Patent 2004/0186. Internat. Classif: B01J C08F B01F, Publication number: 1,015,976A3, (2004).

[12] A. de Broqueville, Rotary fluid bed device and method for using said device, WO2006064046, (2006).

[13] A. de Broqueville, Device and method for injecting fluid into a rotary fluidized bed, WO2008/107404 A1, (2008).

[14] A. de Broqueville, J. De Wilde, Device and method for injecting fluid into a rotating fluidized bed, WO/2007/122211, (2007).

[15] A. de Broqueville, Injectors distributed around a fixed wall of a circular reaction chamber inject fluids along this wall in successive layers; one or more fluids entrain solid particles passing through the chamber in rapid rotation to concentrate them along the wall; for catalytic polymerization, drying, impregnating, US2009/0022632, (2009).

[16] A. de Broqueville, J. De Wilde, Numerical investigation of gas–solid heat transfer in rotating fluidized beds in a static geometry, Chem. Eng. Sci. 64 (6) (2009) 1232–1248, doi:http://dx.doi.org/10.1016/j.ces.2008.11.009.

[17] K. Dewettinck, A. Huyghebaert, Fluidized bed coating in food technology, Trends Food Sci. Technol. 10 (1999) 163–168.

[18] J. De Wilde, A.K. Das, G.H. Heynderickx, G.B. Marin, Development of a transient kinetic model for the simultaneous adsorption of SO_2–NOx over Na/gamma-Al_2O_3 sorbent, Ind. Eng. Chem. Res. 40 (2001) 119–130.

[19] J. De Wilde, Rotating Fluidized Beds in a Static Geometry: From Theory to Industrial Applications, the Prof. Robert Pfeffer seminar, International Fine Particles Research Institute (IFPRI), IFPRI Annual General Meeting 2010. Liège (Château de Colonster), Belgium, June (30) (2010).

[20] J. De Wilde, A. de Broqueville, Rotating fluidized beds in a static geometry: experimental proof of concept, AIChE J. 53 (4) (2007) 793–810, doi:http://dx.doi.org/10.1002/aic.11139.

[21] J. De Wilde, A. Habibi, A. de Broqueville, Experimental and numerical study of rotating fluidized beds in a static geometry, Int. J. Chem. React. Eng. 5 (2007) Article A106.

[22] J. De Wilde, A. de Broqueville, Experimental investigation of a rotating fluidized bed in a static geometry, Powder Technol. 183 (3) (2008) 426–435, doi:http://dx.doi.org/10.1016/j.powtec.2008.01.024.

[23] J. De Wilde, A. de Broqueville, Experimental study of fluidization of 1G-Geldart D-type particles in a rotating fluidized bed with a rotating chimney, AIChE J. 54 (8) (2008) 2029–2044, doi:http://dx.doi.org/10.1002/aic.11532.

[24] J. De Wilde, A. de Broqueville, A rotating chimney for compressing rotating fluidized beds, Powder Technol. 199 (1) (2010) 87–94, doi:http://dx.doi.org/10.1016/j.powtec.2009.04.017.

[25] J. De Wilde, P. Eliaers, A. Poortinga, (FrieslandCampina), A vortex chamber device, and method for treating powder particles or a powder particles precursor, PCT/NL2013/050751 (P99004EP00), (2013).

[26] C. Dodson, Torbed or not Torbed? Chem. Eng.–London 605 (1996) 13–14.

[27] A. Dutta, R.P. Ekatpure, G.J. Heynderickx, A. de Broqueville, G.B. Marin, Rotating fluidized bed with a static geometry: guidelines for design and operating conditions, Chem. Eng. Sci. 65 (5) (2010) 1678–1693.

[28] N.A. Dvornikov, P.P. Belousov, Investigation of a fluidized bed in a vortex chamber, J. Appl. Mech. Tech. Phys. 52 (2) (2011) 206–211.

[29] R. Ekatpure, V.U. Suryawansh, G.J. Heynderickx, A. de Broqueville, G.B. Marin, Experimental investigation of a gas–solid rotating bed ractor with static geometry, Chem. Eng. Process.: Process Intensif. 50 (1) (2011) 77–84.

[30] P. Eliaers, Intensification of interfacial mass, heat, and momentum transfer in high-G fluidized beds in vortex chambers: experimental and theoretical study of potential applications, PhD Thesis, Université catholique de Louvain (UCL), Louvain-la-Neuve, Belgium, 2014.

[31] P. Eliaers, J. De Wilde, Drying of biomass pellets: experimental study and comparison of the performance of a conventional fluidized bed and a rotating fluidized bed in a static geometry, Annual AIChE Meeting, Pittsburgh, USA, October 28–November 2, 2012.

[32] P. Eliaers, J. De Wilde, Wet coating of Geldart-C type particles in a rotating fluidized bed in a static geometry, 2012 Annual AIChE Meeting, Pittsburgh, USA, October 28–November 2, 2012.

[33] P. Eliaers, J. De Wilde, Drying of biomass particles: experimental study and comparison of the performance of a conventional fluidized bed and a rotating fluidized bed in a static geometry, Drying Technol. 31 (2) (2013) 236–245.

[34] P. Eliaers, A. de Broqueville, A. Poortinga, T. van Hengstum, J. De Wilde, High-G, low-temperature coating of cohesive particles in a vortex chamber, Powder Technol. 258 (2014) 242–251.

[35] S. Ergun, Fluid flow through packed columns, Chem. Eng. Prog. 48 (89) (1952).

[36] L.T. Fan, C.C. Chang, Y.S. Yu, T. Takahashi, Z. Tanaka, Incipient fluidization condition for a centrifugal fluidized bed, AIChE J. 31 (1985) 999–1009.

[37] B.A. Folsom, Two-phase flow in vertical and annular fluidized beds, PhD Thesis, California Institute of Technology, 1974.

[38] G.F. Froment, K.B. Bischoff, J. De Wilde, Chemical Reactor Analysis and Design, Wiley Series in Chemical Engineering, third ed., September (2010), ISBN 9780470565414.

[39] D. Gidaspow, Multiphase Flow and Fluidization: Continuum and Kinetic Theory Descriptions, first ed., Academic Press, 1994.

[40] M. Goldshtik, F. Hussain, R.J. Yao, The vortex liquid piston engine and some other vortex technologies, Sādhanā 22 (3) (1997) 323–367.

[41] M.A. Howley, R. Pfeffer, The hydrodynamics of a rotating fluidized bed, Proceedings of AIChE Annual meeting, Cincinnati, OH, 2005.

[42] S.M. Jacob, B. Gross, S.E. Voltz, V.W. Weekman Jr., A lumping and reaction scheme for catalytic cracking, AIChE J. 22 (1976) 701–713.

[43] L.M. Kochetov, B.S. Sazhin, E.A., Karlik, Experimental determination of the optimal ratios of structural dimensions in the whirl chamber for drying granular materials, Khimicheskoe i Neftyanoe Mashinostroenie, 2 (10) (1969).

[44] L.M. Kochetov, B.S. Sazhin, E.A. Karlik, Hydrodynamics and heat exchange in vortex drying chambers, Khimicheskoe i Neftyanoe Mashinostroenie, 9 (10) (1969).

[45] D.G. Kroger, E.K. Levy, J.C. Chen, Flow characteristics in packed and fluidized rotating beds, Powder Technol. 24 (1979) 9–18.

[46] A.O. Kuzmin, M. Pravdina, A.I. Kh Yavorsky, N.I. Yavorsky, V.N. Parmon, Vortex centrifugal bubbling reactor, Chem. Eng. J. 107 (2005) 55–62.

[47] Lewellen W.S., Stickler D.B., Two-Phase Vortex Investigation Related to the Colloidal Core Nuclear Reactor, ARL TR 72-0037, Aerospace Research Laboratory, Wright Patterson Air Force Base, OH, USA, (1972).

[48] P.J. Loftus, D.B. Stickler, R.C. Diehl, A confined vortex scrubber for fine particulate removal from flue gases, Env. Prog. 11 (1) (1992) 27–32.

[49] E.A. Pitsukha, S. Teplitskii Yu, V.A. Borodulya, Investigation of flows in a vortex-bed chamber, J. Eng. Phys. Thermophys. 85 (5) (2012) 1025–1033.

[50] G.-H. Qian, I. Bágyi, R. Pfeffer, H. Shaw, J.G. Stevens, Particle mixing in rotating fluidized beds: inferences about the fluidized state, AIChE J. 45 (1999) 1401–1410.

[51] G.-H. Qian, I. Bagyi, I.W. Burdick, R. Pfeffer, H. Shaw, J.G. Stevens, Gas–solid fluidization in a centrifugal field, AIChE J. 47 (2001) 1022–1034.

[52] J.A. Quevedo, H. Nakamura, Y. Shen, R.N. Dave, R. Pfeffer, Fluidization of nanoparticles in a rotating fluidized bed, AIChE Annual meeting, Cincinnati, OH, USA, 2005.

[53] J. Quevedo, R. Pfeffer, Y. Shen, R. Dave, H. Nakamura, S. Watano, Fluidization of nanoagglomerates in a rotating fluidized bed, AIChE J. 52 (2006) 2401–2412.

[54] J.H. Saunders, Particle entrainment from rotating fluidized beds, Powder Technol. 47 (1986) 211–217.

[55] B.S. Sazhin, L.M. Kochetov, A.S. Belousov, Retention capacities and flow patterns of vortex contactors, Theor. Found. Chem. Eng. 42 (2) (2008) 125–135.

[56] J. Shu, V.I. Lakshmanan, C.E. Dodson, Hydrodynamic study of a toroidal fluidized bed reactor, Chem. Eng. Process. 39 (6) (2000) 499–506.

[57] O. Simonin, E. Deutsch, J.P. Minier, Eulerian prediction of the fluid/particle correlated motion in turbulent two-phase flows, Appl. Sci. Res. 51 (1993) 275–283.

[58] J.J. Smulsky, The weighted layer of particles in the cylindrical vortex chamber, J. Appl. Chem. 8 (1983) 1782–1789.

[59] N. Staudt, A. de Broqueville, W.R. Trujillo, J. De Wilde, Low-temperature pyrolysis and gasification of biomass: numerical evaluation of the process intensification potential of rotating- and circulating rotating fluidized beds in a static fluidization chamber, Int. J. Chem. Reactor Eng. 9 (2011) Paper A43.

[60] D.B. Stickler, H. Lakshmikantha, W.S. Lewellen, Heat Transfer and Containment Processes in Two-Phase Cavity Nuclear Reactor, ARL TR 74-0007, Aerospace Research Laboratory, Wright Patterson Air Force Base, OH, USA, 1974.

[61] E. Teunou, D. Poncelet, Fluid-bed coating, in: C. Onwulata (Ed.), Encapsulated and Powdered Foods, Taylor & Francis, Boca Raton, FL, 2005, pp. 197–212.

[62] W.R. Trujillo, J. De Wilde, Computational fluid dynamics simulation of fluid catalytic cracking in a rotating fluidized bed in a static geometry, Ind. Eng. Chem. Res. 49 (11) (2010) 5288–5298, doi:http://dx.doi.org/10.1021/ie901610f.

[63] W.R. Trujillo, J. De Wilde, Experimental study of the fluidization of Geldart A type catalyst in a rotating fluidized bed in a static geometry, AIChE Annual Meeting, Minneapolis, Minnesota, USA, October 16–21, 2011.

[64] W.R. Trujillo, M. Abouahi, J. De Wilde, Design aspects of rotating fluidized beds in a static fluidization chamber, XIIIeme Congrès de la Société Française de Génie des Procédés (SFGP 2011). Lille, France, November 29–December 1, (2011).

[65] W.R. Trujillo, J. De Wilde, Fluid catalytic cracking in a rotating fluidized bed in a static geometry: a cfd analysis accounting for the distribution of the catalyst coke content, Powder Technol. 221 (2012) 36–46, doi:http://dx.doi.org/10.1016/j.powtec.2011.12.015.

[66] R. Turton, X.X. Cheng, The scale-up of spray coating processes for granular solids and tablets, Powder Technol. 150 (2) (2005) 78–85.

[67] G.H. Vatistas, S. Lin, C.K. Kwok, Theoretical and experimental studies on vortex chamber flows, AIAA J. 24 (4) (1986) 635–642.

[68] E.P. Volchkov, V.I. Terekhov, A.N. Kaidanik, A.N. Yadykin, Aerodynamics and heat and mass transfer of fluidized particle beds in vortex chambers, Heat Transfer Eng. 14 (3) (1993) 36–47.

[69] E.P. Volchkov, N.A. Dvornikov, A.N. Yadykin, Characteristic features of heat and mass transfer in a fluidized bed in a vortex chamber, Heat Transfer Res. 34 (7–8) (2003) 486–498.

[70] E.P. Volchkov, N.A. Dvornikov, V.V. Lukashov, R.Kh. Abdrakhmanov, The experimental study of heat- mass transfer and flow field in the vortex chamber with centrifugal fluidized bed, 14th International Conference on Methods of Aerophysical Research (ICMAR 2008), Akademgorodok, Novosibirsk, Russia, June 30–July 6, 2008.

[71] E.P. Volchkov, N.A. Dvornikov, V.V. Lukashov, R. Abdrakhmanov, Investigation of the flow in the vortex chamber with centrifugal fluidized bed with and without combustion, Thermophys. Aeromech. 20 (6) (2013) 663–668.

[72] S. Watano, H. Nakamura, K. Hamada, Y. Wakamatsu, Y. Tanabe, R.N. Dave, R. Pfeffer, Fine particle coating by a novel rotating fluidized bed coater, Powder Technol. 141 (2004) 172–176.

[73] S. Watano, Y. Imada, K. Hamada, Y. Wakamatsu, Y. Tanabe, R.N. Dave, R. Pfeffer, Microgranulation of fine powders by a novel rotating fluidized bed granulator, Powder Technol. 131 (2003) 250–255.

[74] G.A. Wellwood, Hydrodynamic behaviour of the Torbed reactor operating in fine particle mode, PhD Thesis, University of Queensland, 2000.

[75] S.R.L. Werner, J.R. Jones, A.H.J. Paterson, R.H. Archer, D.L. Pearce, Air-suspension particle coating in the food industry: part I – state of the art, Powder Technol. 171 (2007) 25–33.